

Acoustic wave generation in collapsing massive stars with convective shells

Ernazar Abdikamalov¹[★] and Thierry Foglizzo²[†]

¹*Department of Physics, Nazarbayev University, Nur-Sultan 010000, Kazakhstan*

²*AIM, CEA, CNRS, Université Paris-Saclay, Université Paris Diderot, Sorbonne Paris Cité, F-91191 Gif-sur-Yvette, France*

Accepted XXX. Received YYY; in original form ZZZ

ABSTRACT

The convection that takes place in the innermost shells of massive stars plays an important role in the formation of core-collapse supernova explosions. Upon encountering the supernova shock, additional turbulence is generated, amplifying the explosion. In this work, we study how the convective perturbations evolve during the stellar collapse. Our main aim is to establish their physical properties right before they reach the supernova shock. To this end, we solve the linearized hydrodynamics equations perturbed on a stationary background flow. The latter is approximated by the spherical transonic Bondi accretion, while the convective perturbations are modeled as a combination of entropy and vorticity waves. We follow their evolution from large radii, where convective shells are initially located, down to small radii, where they are expected to encounter the accretion shock above the proto-neutron star. Considering typical vorticity perturbations with a Mach number ~ 0.1 and entropy perturbations with magnitude $\sim 0.05k_b/\text{baryon}$, we find that the advection of these perturbations down to the shock generates acoustic waves with a relative amplitude $\delta p/\gamma p \lesssim 10\%$, in agreement with published numerical simulations. The velocity perturbations consist of contributions from acoustic and vorticity waves with values reaching $\sim 10\%$ of the sound speed ahead of the shock. The perturbation amplitudes decrease with increasing ℓ and initial radii of the convective shells.

Key words: Accretion – Hydrodynamics – Instabilities – Shock waves

1 INTRODUCTION

The strong convection that massive stars develop in their innermost nuclear-burning shells are expected to play an important role in their explosions (e.g., Couch et al. 2015; Müller et al. 2017). Following the collapse of the iron core, the convective perturbations descend from their initial position at $\gtrsim 1500$ km towards the center of the star. The supernova shock, launched at core bounce, encounters these perturbations at a radius of ~ 150 km within $\sim 200 - 300$ ms after formation (or within $\sim 400 - 500$ ms after the start of the iron core collapse) (e.g., Müller & Janka 2015; Müller 2016). The interaction of the two amplifies the violent non-radial motion in the post-shock region, generating an additional pressure behind the shock and thus creating a more favorable condition for producing an explosion (Couch & Ott 2013; Couch et al. 2015; Takahashi et al. 2016; Müller et al. 2017; Nagakura et al. 2019). The oxygen-burning and, to a lesser extent, the silicon-burning shells are expected to

have a particularly strong impact on the explosion condition (Collins et al. 2018).

During their accelerated infall towards the shock, the convective perturbations undergo profound evolution, as revealed by multi-dimensional numerical simulations (Buras et al. 2006; Müller & Janka 2015; Couch et al. 2015; Müller et al. 2017) as well as semi-analytical (Takahashi & Yamada 2014) and analytical calculations (Kovalenko & Eremin 1998; Lai & Goldreich 2000). The density of the collapsing shells increases as they descend towards the center. The infall velocity gradually increases, becoming supersonic in the inner part of the flow. The shrinking convective vortices spin up due to the conservation of angular momentum. In addition, the convective eddies have to constantly adjust to new pressure balance, a process that generates strong acoustic waves (e.g., Foglizzo 2001). When these perturbations arrive ahead of the supernova shock, their physical properties affect the way they interact with the shock (Abdikamalov et al. 2016; Abdikamalov et al. 2018; Huete et al. 2018; Huete & Abdikamalov 2019; Radice et al. 2018).

The aim of our work is to shed some light on the physical properties of the convective perturbations right before

[★] E-mail: ernazar.abdikamalov@nu.edu.kz

[†] E-mail: foglizzo@cea.fr

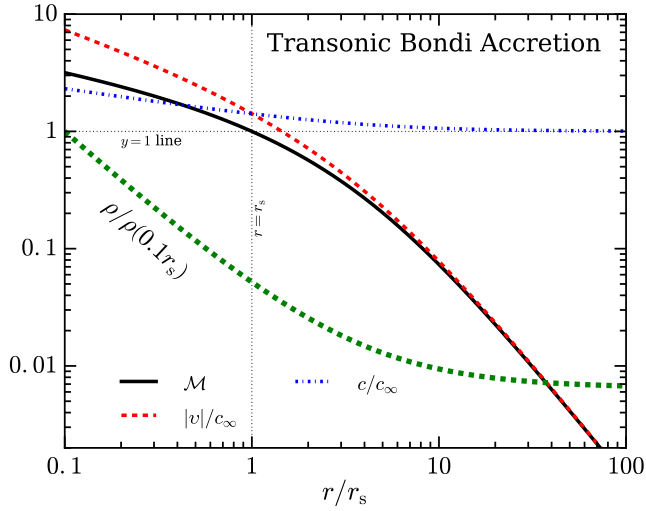


Figure 1. Transonic Bondi solution as a function of radius for $\gamma = 4/3$. The thick black lines shows the Mach number of the flow, while the dashed thick red line shows the advection velocity in units of c_∞ . The sound speed is shown with dashed-dotted blue line. For reference, the thin vertical dotted line shows the location of the sonic point $r = r_s$, while the thin horizontal dotted line shows the ordinate $y = 1$.

they reach the supernova shock. We treat the convective perturbations as a combination of vorticity and entropy waves co-moving with the mean flow. We evolve the perturbations using an extension of the linear hydrodynamics formalism of Foglizzo (2001). Our work improves on previous studies in a number of ways. We follow the evolution of the perturbations starting from their initial location at $\gtrsim 1.5 \times 10^3$ km down to regions with radii ~ 150 km where they are expected to encounter the supernova shock. Thus, we go beyond the $r \rightarrow 0$ asymptotic limit used in the previous works (Kovalenko & Eremin 1998; Lai & Goldreich 2000). In addition, the simplicity of our method allows us to obtain an additional insight into the physics of the process compared to three-dimensional numerical simulations (Couch et al. 2015; Müller et al. 2017). In particular, we establish the physical constituents of the perturbations – the vorticity, entropy, and acoustic waves – and calculate their properties.

The paper is organized as following. We present the method in Section 2. The results are presented in Section 3. The conclusion is provided in Section 4.

2 METHOD

We solve the linearized hydrodynamics equations for advected convective perturbations on a stationary background flow. The stellar matter is modeled using an ideal gas equation of state with an adiabatic index $\gamma = 4/3$. In order to check the sensitivity of our results to the value of γ , we perform additional calculations for $\gamma = 1.5$ and we find qualitatively similar results. We assume that the background flow is given by the stationary spherical transonic Bondi solution (Bondi 1952). The radial profiles of velocity, speed of sound, density, and Mach number are shown in Fig. 1. The mean flow speed increases with decreasing r . While the Bondi so-

lution represents an approximation to the flow in realistic stars (e.g., it assumes uniform composition and neglects the time-dependence of the collapse), its simplicity allows us to obtain a unique and deep insight into the physics of the advection of the perturbations. The flow is subsonic (supersonic) above (below) the sonic radius r_s ,

$$r_s = \frac{5 - 3\gamma}{4} r_B, \quad (1)$$

where r_B is the Bondi radius GM/c_∞^2 and c_∞ is the sound speed at infinity, which is a free parameter in our model. Due to the stationarity of the background flow, the mass of the accretor M is assumed to be constant in our model. That said, all the results that we present in this work are independent of the values of M and c_∞ . At the sonic point r_s , the flow velocity equals the local sound speed,

$$c_s = \left(\frac{2}{5 - 3\gamma} \right)^{\frac{1}{2}} c_\infty. \quad (2)$$

For $\gamma = 4/3$, the sound speed at the sonic point equals $\sqrt{2}c_\infty$. Details of the Bondi solution are described in the Appendix A of Foglizzo (2001).

We model convective perturbations as a combination of vorticity and entropy waves. Since the convection in nuclear-burning shells is subsonic (e.g., Kippenhahn et al. 2013), the contribution of acoustic waves is considered negligible before collapse (Lighthill 1952; Lighthill 1954; Goldreich & Kumar 1990). We also neglect internal gravity waves in our model. While g-modes are expected to play an important role in stellar evolution (e.g., Quataert & Shiode 2012; Fuller 2017) and may affect the final spin of the stellar core (Fuller et al. 2015), their impact on the explosion condition of CCSNe are expected to be rather minor (Müller et al. 2017).

We decompose the velocity field of hydrodynamic perturbations into vector spherical harmonics (e.g., Chatzopoulos et al. 2014; Kovalenko & Eremin 1998)

$$\begin{aligned} \delta \mathbf{v}(r, t, \theta, \phi) = & \left\{ \delta v_r(r) Y_{\ell m} \hat{\mathbf{r}} \right. \\ & + \delta v_\perp(r) L^{-1} \hat{\mathbf{v}}_\perp Y_{\ell m} \\ & \left. + \delta v_{\text{rot}}(r) L^{-1} \hat{\mathbf{v}}_\perp Y_{\ell m} \times \hat{\mathbf{r}} \right\} e^{-i\omega t}, \end{aligned} \quad (3)$$

where ω is the angular frequency, $\hat{\mathbf{r}}$, $\hat{\boldsymbol{\theta}}$, and $\hat{\boldsymbol{\phi}}$ are unit vectors and

$$\hat{\mathbf{v}}_\perp = \hat{\boldsymbol{\theta}} \frac{\partial}{\partial \theta} + \hat{\boldsymbol{\phi}} \frac{1}{\sin \theta}. \quad (4)$$

The normalization factor $L = (\ell(\ell + 1))^{1/2}$ is introduced to account for the asymptotic amplitude of the angular derivative of the spherical harmonic $Y_{\ell m}$. We show in Appendix D that the horizontal component $\delta v_{\text{rot}}(r)$ fully accounts for the vertical component of vorticity. In the linear approximation, $\delta v_{\text{rot}}(r)$ decouples from the rest of the flow and scales as $\propto r^{-1}$, as dictated by the conservation of angular momentum. The radial and transverse components $\delta v_r(r)$ and $\delta v_\perp(r)$ are responsible for the horizontal components of the vorticity vector as well as acoustic waves.

For adiabatic flows, the entropy variations are conserved and "frozen into" the mean flow. The amplitude of vorticity

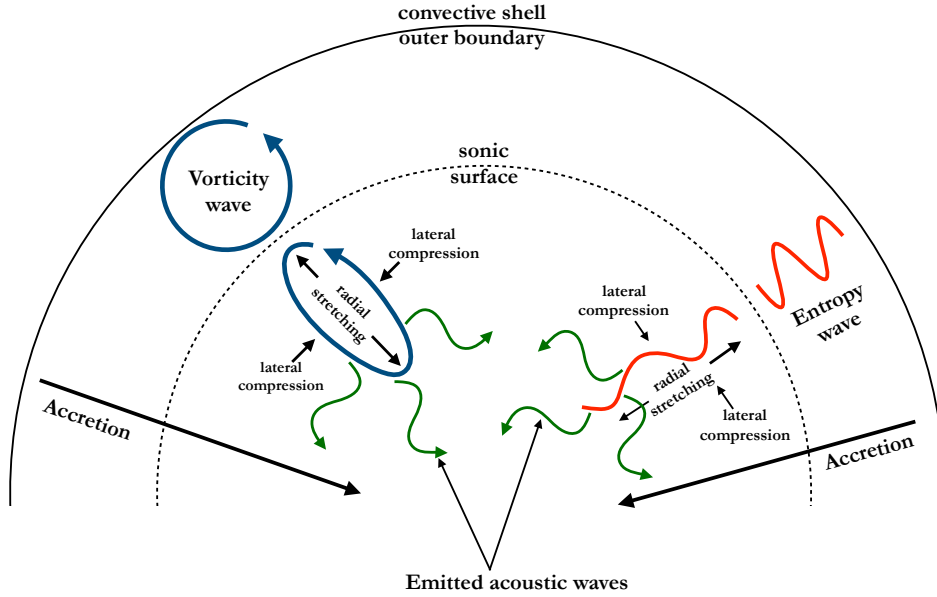


Figure 2. Approximate schematic depiction of horizontal vorticity and entropy waves in convective shells of a collapsing star. During the collapse, these perturbations are advected towards the center together with the flow. The contraction of the waves generates pressure perturbations that travel as acoustic waves. The contracting entropy waves generate additional vorticity via the baroclinic effect. At large radii, the infall velocity is small, but as the collapse progresses down to small radii, the infall speed accelerates (cf. Fig 1) and becomes supersonic. The sonic surface is shown with the dashed semi-circle. The entropy and vorticity perturbations are radially stretched by the acceleration. Note that both vorticity and entropy waves couple to pressure perturbations even while traveling in the subsonic region, but their amplitude is much smaller and hence it is not depicted here for the clarity of the illustration.

perturbations $\delta\omega \equiv \nabla \times \delta\mathbf{v}$ is affected by advection and by entropy perturbations in such a way that the quantity δK defined in Foglizzo (2001) is linearly conserved and acts as a source for the generation of sound waves (cf. Appendix D):

$$\delta K \equiv r^2 \mathbf{v} \cdot (\nabla \times \delta\omega) + L^2 c^2 \frac{\delta S}{\gamma}, \quad (5)$$

where δS is the dimensionless entropy, the value of which equals the entropy per baryon in the units of Boltzmann constant k_b , as shown in Appendix E. Following Foglizzo (2001), we model both perturbations as sinusoidal waves with frequency ω that are advected with the mean flow. Thus, the incoming perturbations are characterized by only four quantities: the amplitudes $|\delta K|$ and $|\delta S|$ associated to the frequency ω and the angular wavenumber ℓ .

We formulate the linear hydrodynamics equations in a compact form using the function $\delta\tilde{f}$, which is related to the perturbations of the Bernoulli constant of the flow (cf. Appendix A):

$$\frac{\partial^2 \delta\tilde{f}}{\partial X^2} + W\delta\tilde{f} = A\delta S_R + B\delta K_R \quad (6)$$

where the variable X is related to r via Eq. (A23), while the functions W , A , and B are related to the properties of the background flow as well as the frequency ω and wavenumber ℓ of the perturbations (cf. eqs. A24-A25). The quantities δS_R and δK_R are set by the amplitudes of entropy and horizontal vorticity perturbations at the radius R . Thus, the solution of the equation is linearly proportional to the am-

plitude of the source terms δS_R and δK_R . The homogeneous part of Eq. (6) describes freely propagating acoustic waves. The general solution of Eq. (6) is obtained in Appendices A-C using Green functions and the regularity condition at the sonic point. A second-order Frobenius expansion is necessary to smoothly connect the solutions in the subsonic and supersonic regions. Far from the accretor, the identification of ingoing and outgoing waves using the WKB approximation allows us to define the outer boundary condition as the absence of incoming acoustic waves from infinity. We set the outer boundary at $40r_s$, which is sufficiently far away for the WKB approximation to be valid (cf. Appendix B). An additional condition follows from the requirement of the regularity of the solution at the sonic point. The numerical solutions of the homogeneous equation are obtained using an implicit Runge-Kutte method.

The angular wavenumber of the dominant mode is largely determined by the size of the shell relative to its radius (Chandrasekhar 1961; Foglizzo et al. 2006):

$$\ell \sim \frac{\pi}{2} \frac{r_+ + r_-}{r_+ - r_-}, \quad (7)$$

where r_+ and r_- are the outer and inner boundaries of the convective shell. Modes with ℓ ranging from 1 to ~ 100 have been observed in numerical simulations (Collins et al. 2018), but the impact of large- ℓ modes on the explosion condition of CCSNe are expected to be rather limited (Müller et al. 2016; Kazeroni & Abdikamalov 2019). Assuming that the dominant mode with wavenumber ℓ spans the entire radial

extent of the convective zone, the radial size $\Delta R = r_+ - r_-$ is related to ℓ using Eq. (7):

$$\Delta R = \frac{\pi}{\ell} \frac{r_+ + r_-}{2} = \frac{\pi}{\ell} R_{\text{shell}}, \quad (8)$$

where R_{shell} is interpreted as the radius of the convective vortices before collapse. The value of R_{shell} is different for different stellar models (e.g., Collins et al. 2018). For this reason, we treat R_{shell} as a free parameter. In our model, this corresponds to a radius at which the vortex has a circular shape. For the Bondi flow, this condition can be expressed as $R_{\text{shell}} = Lv(R_{\text{shell}})/\omega$, where $v(R_{\text{shell}})$ is the advection velocity at $r = R_{\text{shell}}$. In our study, we consider 4 values of R_{shell} ranging from r_s to $4r_s$, keeping in mind that $r_s \sim 2,000 - 3,000$ km within $\sim 100 - 300$ ms after bounce, a time span within each CCSN shock is expected to encounter the convective perturbations. As we will see below, these values of R_{shell} cover the parameter space of the perturbations that are likely to have the strongest impact on the explosion condition of CCSNe.

Numerical simulations predict convective Mach numbers $\lesssim 0.1$ in the innermost shells (Müller et al. 2016; Collins et al. 2018; Yadav et al. 2019; Yoshida et al. 2019), while the associated entropy fluctuations are $\lesssim 0.05 k_b/\text{nucleon}$ (e.g., Meakin & Arnett 2007). In our calculations, we normalize entropy perturbations to $0.05 k_b/\text{baryon}$. For horizontal vorticity perturbations, we choose the normalization factor, i.e. $|\delta K|$, to yield a convective Mach number of 0.1 at the pre-collapse locations of the convective vortices. Since the shell convection in massive stars is driven by buoyancy, the vertical vorticity is expected to be smaller than the horizontal component. This is supported by the study of Chatzopoulos et al. (2014), who performed the decomposition of convective velocities in massive stars into vector spherical harmonics. At peak ℓ , their parameter β , which measures the horizontal circulation, is smaller by a factor of a few than their measure of vertical circulation γ (cf. Fig. 13 of Chatzopoulos et al. (2014)). In our study, we conservatively assume that the Mach number of the horizontal circulation is $\delta v_{\text{rot}} = 10^{-2}$, i.e., an order of magnitude smaller than that of the vertical circulation. We point out that, while the precise values of δv_{rot} , δK , and δS are likely to depend on the properties of specific stellar models (e.g., Collins et al. 2018), our formalism is linear with respect to δv_{rot} , δK , and δS . Hence, our results can simply be scaled linearly to other values of these parameters. This allows us to capture any value of the convective Mach numbers and entropy fluctuations.

In summary, the values of $|\delta K|$ and $|\delta S|$ as well as ℓ and the initial radius R_{shell} of convective vortices fully specify the physical properties of the convective perturbations which couple to the pressure field in our model.

3 RESULTS

3.1 Qualitative picture

The production of pressure perturbations from the advection of horizontal vorticity perturbations can be understood by considering a vorticity perturbation $\delta\omega$ with a characteristic size δr in a collapsing star. As it moves together with the converging mean flow, this perturbation distorts the iso-density surfaces of the flow and induces a density change

(Foglizzo 2001; Müller & Janka 2015). This density change is associated with pressure perturbation $\delta p/\gamma p \sim \delta\rho/\rho$. To an order of magnitude,

$$\frac{\delta p}{\gamma p} \sim \frac{\delta\rho}{\rho} \sim \frac{\partial \ln \rho}{\partial \ln r} \frac{\delta r}{r} \quad (9)$$

where ρ is the mean density and p is the mean density of the background flow. The displacement δr is related to the radial velocity perturbations via $\delta r \sim 2\pi\delta v_r/\omega$, where ω is the angular frequency of the perturbation. The radial velocity perturbation δv_r is related to the perturbed vorticity $\delta\omega$ via $\delta\omega \sim im\delta v_r/r$, where m is the angular order of the perturbation. Combining these, we obtain

$$\frac{\delta p}{\gamma p} \sim \frac{\partial \ln \rho}{\partial \ln r} \frac{2\pi\delta\omega}{im\omega}. \quad (10)$$

The pressure perturbation $\delta p/\gamma p$ is thus expected to be largest for small m , i.e., for large-scale perturbations (Foglizzo 2009; Müller & Janka 2015). In the limit of a uniform flow ($\partial \ln \rho/\partial \ln r = 0$), the advection of vorticity perturbations does not emit acoustic waves as expected (Kovaszny 1953). Note that the emission of sound by advected horizontal vorticity can also be explained using the shallow water analogy (Foglizzo et al. 2015). The vertical component of vorticity does not couple to the pressure field.

The production of pressure perturbations from the advection of entropy perturbations can be understood by considering a fluid element of mass m with a perturbed entropy δs . The expansion of a gas element under an adiabatic change of pressure depends on its entropy. The corresponding change of volume induces the emission of acoustic waves. When the fluid element is advected from a region with mean specific enthalpy h_1 to another region with mean specific enthalpy h_2 , the energy of the emitted acoustic waves is deduced from energy conservation (Foglizzo & Tagger 2000)

$$\delta E = (h_2 - h_1) \delta m, \quad (11)$$

where

$$\delta m = m \frac{\delta\rho}{\rho} = m \frac{\delta s}{\gamma c_v} \quad (12)$$

is the the variation of the mass m of the fluid element with same volume and perturbed entropy δs and c_v is the specific heat at constant volume. From this, we can obtain the total specific energy of emitted acoustic waves (Foglizzo & Tagger 2000):

$$\delta \mathcal{E} \sim (h_2 - h_1) \frac{\delta s}{\gamma c_v}. \quad (13)$$

Thus, the energy of sound waves is proportional to the entropy change δs and to the variation $h_2 - h_1$, of the enthalpy. No acoustic waves are emitted if the flow is uniform ($h_2 = h_1$). A schematic depiction of the process is presented in Fig. 2.

In addition, if the entropy perturbations have a transverse structure, the surfaces of constant pressure do not coincide with those of constant density. The net pressure force on a fluid element does not pass through its center of mass. This baroclinic effect creates a net torque on the fluid element, generating additional vorticity (e.g., Thorne & Blandford 2017) as illustrated by Eqs. (D6, D7) in Appendix D.

3.2 Evolution of vorticity

We now discuss how vorticity perturbations evolve during their advection towards the center. This includes not only the vorticity perturbations originating in convective shells, but also the vorticity generated by the advected entropy perturbations due to the baroclinic effect. After establishing the behavior of the vorticity perturbations, we will discuss the acoustic waves emitted by the advected horizontal vorticity and entropy perturbations (Section 3.3).

As mentioned above, the velocity perturbation associated with the vertical component of vorticity evolves as $\propto r^{-1}$ (Kovalenko & Eremin 1998). It is linearly decoupled from the rest of the perturbations and it does not depend on ℓ . Depending on the initial radius, δv_{rot} may amplify by a factor of $\gtrsim 10$ when they reach $r \sim 0.1r_s$, which is approximately the radius where the stalled CCSN shock is expected to encounter these perturbations. The dashed lines on the left panel of Fig. 3 shows $\delta v_{\text{rot}}/c$ as a function of r for different values of the initial radius R_{shell} . The Mach number of horizontal motions associated to the vertical vorticity scales as $\delta v_{\text{rot}}/c \sim 0.06(R_{\text{shell}}/r_s)^{0.9}$. For most values of R_{shell} , δv_{rot} becomes $\sim 10^{-1}$ in the inner regions of the flow.

The evolution of the horizontal vorticity is drastically different from that of the vertical component. The total velocity δv associated to the horizontal vorticity, defined as $(\delta v_r^2 + \delta v_\perp^2)^{0.5}$ and shown on the left panel of Fig. 3, decreases with radius starting from $r = R_{\text{shell}}$. This decrease is caused by the stretching of vortex sheets in the radial direction by the accelerated mean flow. As the perturbation advects towards the center, its innermost point travels a longer distance than its outermost point. For this reason, the radial stretching increases more as the perturbation advects further down to smaller radii. The circulation of the vortex lines, defined as integral of velocity over a closed curve,

$$\Gamma = \oint v ds, \quad (14)$$

is a conserved quantity when the entropy is uniform (e.g., Landau & Lifshitz 1959). As the length of the closed curve increases due to the stretching of vortex sheets, the velocity along this curve has to decrease as observed in our calculations. Note that this effect is less pronounced for modes with small R_{shell} , which we can see from the fact that velocities are larger for smaller R_{shell} at $r \lesssim r_s$ (cf. left panel of Fig. 3). This is not surprising as the modes with small R_{shell} have smaller radial sizes and thus are less stretched by the flow in the radial direction. Due to the radial stretching, the radial component of velocity becomes larger than the tangential component, as we can see on the left panel of Fig. 3. On the other hand, at large radii, the vortices are squeezed in the radial direction, and the tangential velocities dominate. Note that the velocities of the advected horizontal vorticity waves, once normalized to yield a Mach number of 0.1 at $r = R_{\text{shell}}$, do not depend on ℓ .

An asymptotic analysis reveals that $\delta v_r \propto r^{1/2}$ and $\delta v_\perp \propto r^2$ in the limit $r \rightarrow 0$ (cf. Appendix F). Thus, the horizontal vorticity perturbations are expected to have a small velocity in this limit, while the vertical vorticity is expected to dominate due to the $\delta v_{\text{rot}} \propto 1/r$ scaling. This result is in disagreement with Kovalenko & Eremin (1998), who find that $\delta v_r/c \propto r^{(3-3\gamma)/4}$ and $\delta v_\perp/c \propto r^{(3\gamma-7)/4}$ in the same limit, which results in $\delta v_r \propto r^{-1/2}$ and $\delta v_\perp \propto r^{-1}$ for $\gamma = 4/3$.

Their scaling appears to be valid for acoustic waves emitted by vorticity waves, not for the vorticity waves themselves (I. Kovalenko, private communication). This conclusion is supported by the fact that a similar scaling was obtained for acoustic waves for $r \rightarrow 0$ by Lai & Goldreich (2000).

The advected entropy waves generate horizontal vorticity due to the baroclinic effect, as mentioned above in Section 3.1. Figure 4 shows the radial profile of $\delta v_\perp/c$ and $\delta v_r/c$ associated to the horizontal vorticity for different values of R_{shell} . As with the advected vorticity waves, these velocities do not depend on ℓ . Since the vortices are generated in radially-accelerated flow, the radial component dominates the transverse component, especially at small radii. An asymptotic analysis reveals that the tangential velocity decreases as $\delta v_\perp \propto r^{3/2}$ while the radial component approaches a constant value, $\delta v_r \sim 10^{-2}$ in the limit $r \rightarrow 0$ (cf. Appendix F). Thus, unlike the horizontal vorticity waves coming from convective shells, the vorticity generated by advected entropy waves has non-zero radial velocity even at $r \rightarrow 0$. This is due to the fact that advected entropy waves continue to produce vorticity, through the baroclinic effect, even in the limit of small r .

3.3 Acoustic perturbations

As the entropy and horizontal vorticity perturbations are advected towards the center, they generate acoustic waves due to the loss of pressure equilibrium with their surrounding. While in Section 3.1 we derived basic qualitative estimates, below we provide more quantitative results obtained by numerical integration of the differential system of perturbed equations (Appendix C).

Figure 5 shows the radial profiles of $|\delta p/\gamma p|$ generated by advected horizontal vorticity (black line) and entropy waves (blue line) with $\ell = 2$ for two different values of R_{shell} : r_s (left panel) and $2r_s$ (right panel). Due to its smaller size, the model with $R_{\text{shell}} = r_s$ undergoes less radial stretching than the model with $R_{\text{shell}} = 2r_s$. As a result, the former model reaches stronger pressure perturbations of ~ 0.1 in the inner regions of the flow, while the latter remains below $\sim 4 \times 10^{-2}$. For both models, the contributions of the advected entropy waves (blue lines) is about an order of magnitude smaller than that of advected horizontal vorticity waves. We find that this is common for perturbations with low $\ell = 1$ and $\ell = 2$, while for larger ℓ the contributions of both perturbations become comparable. The pressure perturbations experience little growth from R_{shell} to $0.1r_s$. This is different from the power-law dependence on radius obtained by Kovalenko & Eremin (1998) and Lai & Goldreich (2000) in the $r \rightarrow 0$ limit. Instead, it resembles a wave-like pattern observed in Takahashi & Yamada (2014) (cf. their Fig. 5). We hypothesize that this behavior is caused by the interference between ingoing and outgoing acoustic waves, forming a pattern similar to standing waves. However, we cannot verify this rigorously because the decomposition into out-going and in-going acoustic waves is not possible for non-uniform flow. In principle, this can be done using the WKB approximation (cf. Appendix F), but this approximation is accurate only in the outer region where the characteristic scale of the flow becomes larger than the size of the perturbations.

At large radii ($r > R_{\text{shell}}$), both models exhibit out-going acoustic waves due to the refraction of in-going radiation

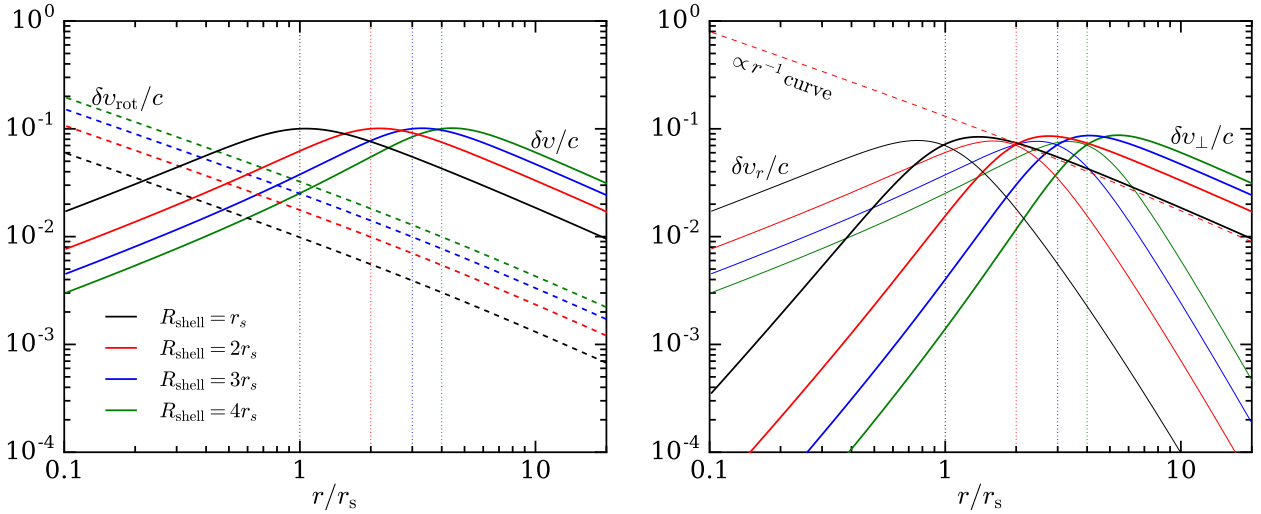


Figure 3. **Left panel:** Mach number $\delta v/c$ of the advected horizontal vorticity waves as a function of radial coordinate r for different values of the initial radii R_{shell} of the convective vortices. δv is defined as $(\delta v_r^2 + \delta v_\perp^2)^{0.5}$. **Right panel:** Mach number of the transverse (think lines) and radial (thin lines) components of the velocity field of the advected horizontal vorticity waves as a function of r for different values of R_{shell} . The velocities are deduced from Eqs. (F9) and (F10). The normalization factor for horizontal vorticity waves is chosen in such a way as to yield convective Mach number of 0.1 at the pre-collapse location of the convective vortices R_{shell} . The component $\delta v_{\text{rot}}/c$, responsible for the vertical vorticity, is assumed to be 10^{-2} at $r = R_{\text{shell}}$.

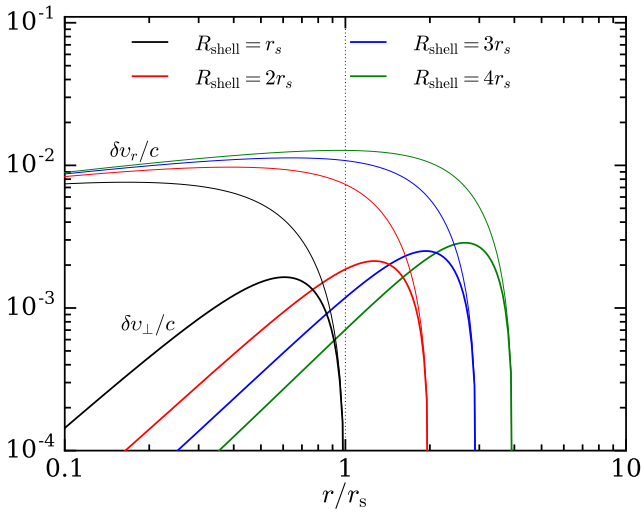


Figure 4. Mach number $\delta v/c$ of the transverse (thick lines) and radial components (thin lines) of the velocity field of horizontal vorticity perturbations generated by advected entropy fluctuations with $\delta S = 0.05$ for different values of R_{shell} . The velocities are deduced from Eqs. (F11) and (F12).

(Foglizzo 2001). The outgoing acoustic waves exhibit the $\propto r^{-1}$ scaling shown by the dotted red line, which is a simple consequence of the conservation of energy. The perturbation with $R_{\text{shell}} = 2r_s$ exhibits significantly stronger out-going radiation than the model with $R_{\text{shell}} = r_s$. This is an expected behavior as waves with larger wavelength undergo stronger refraction Foglizzo (2001).

It is interesting to contrast the behavior of the pressure perturbations with that of velocity perturbations. The dashed and dotted lines in Fig. 5 show $\delta v_r/c$ and $\delta v_\perp/c$. In the supersonic region ($r < r_s$), both quantities are compara-

ble to the value of $\delta p/\gamma p$ as expected for sound waves (e.g., Landau & Lifshitz 1959). This suggests that the velocity field at small radius is mostly due to acoustic waves. At large radius ($r \gtrsim r_s$), the situation depends on the perturbation parameters. For the perturbation with $R_{\text{shell}} = 2r_s$, as discussed above, there is significant amount of out-going acoustic waves. In this case, we have $\delta v_r/c \sim \delta p/\gamma p$, as expected for acoustic waves. However, the transverse component is larger than the radial component by about an order of magnitude because, at large radii, the vertical vortices become squeezed in the radial direction and thus develop strong non-radial velocities. For perturbation with $R_{\text{shell}} = r_s$, both $\delta v_r/c$ and $\delta v_\perp/c$ become significantly larger than $\delta p/\gamma p$. The reason for this behavior is that the velocity field at large radius is dominated by the contribution of vorticity waves only, while the contribution of acoustic waves is negligible. This weak advective-acoustic coupling at large radius is a consequence of the uniform character of the flow within distances comparable to the size of the perturbations. As in the case of pressure perturbations, the contribution of the advected entropy waves to $\delta v_r/c$ and $\delta v_\perp/c$, shown with blue dashed and dotted lines in Fig. 5, is a factor ~ 10 smaller than the contribution of advected vorticity perturbations.

Next we analyze the behavior of $\delta p/\gamma p$ at $0.1r_s$ generated the advected entropy and vertical vorticity perturbations¹, which is shown on the left panel of Fig. 6 for different values of ℓ and R_{shell} . For small values of $\ell = 1$ and $\ell = 2$ or for $r = R_{\text{shell}}$, we find that $|\delta p/\gamma p| \sim 0.1$, in agreement with the results of 3D numerical simulations (Müller et al. 2017). The pressure perturbations decreases with increasing ℓ , in agreement with the qualitative estimate (10). It also decreases with increasing R_{shell} , becoming $\lesssim 10^{-3}$ for $R_{\text{shell}} = 4r_s$ and $\ell \gtrsim 4$. This is caused by the fact that the

¹ We superpose the pressure contributions of entropy δp_e and vorticity waves δp_k as $\delta p = (\delta p_e^2 + \delta p_k^2)^{0.5}$.

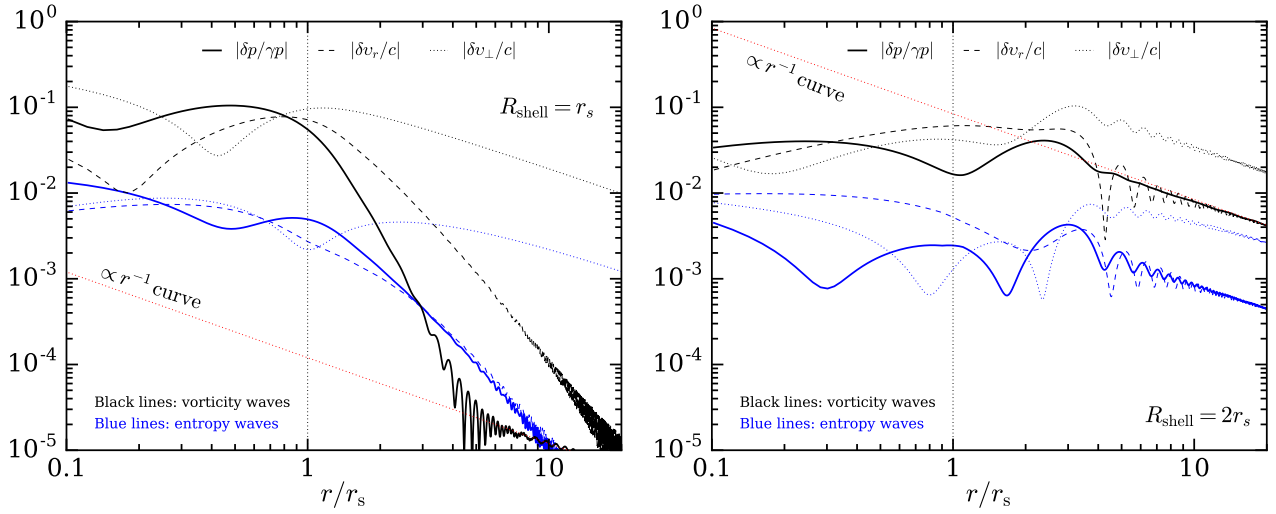


Figure 5. Pressure perturbations for incoming horizontal vorticity (thick black lines) and entropy (thick blue lines) waves with $\ell = 2$ and $R_{\text{shell}} = r_s$ (left panel) and $R_{\text{shell}} = 2r_s$ (right panel), deduced from Eq. (A13). The dashed (dotted) lines show the amplitude of the radial velocity fluctuations $|\delta v_r/c|$ (tangential velocity fluctuations $|\delta v_\perp/c|$) for incoming horizontal vorticity and entropy waves. The vertical dashed line shows the location of the sonic point, while the dotted red line shows the $\propto r^{-1}$ slope for reference.

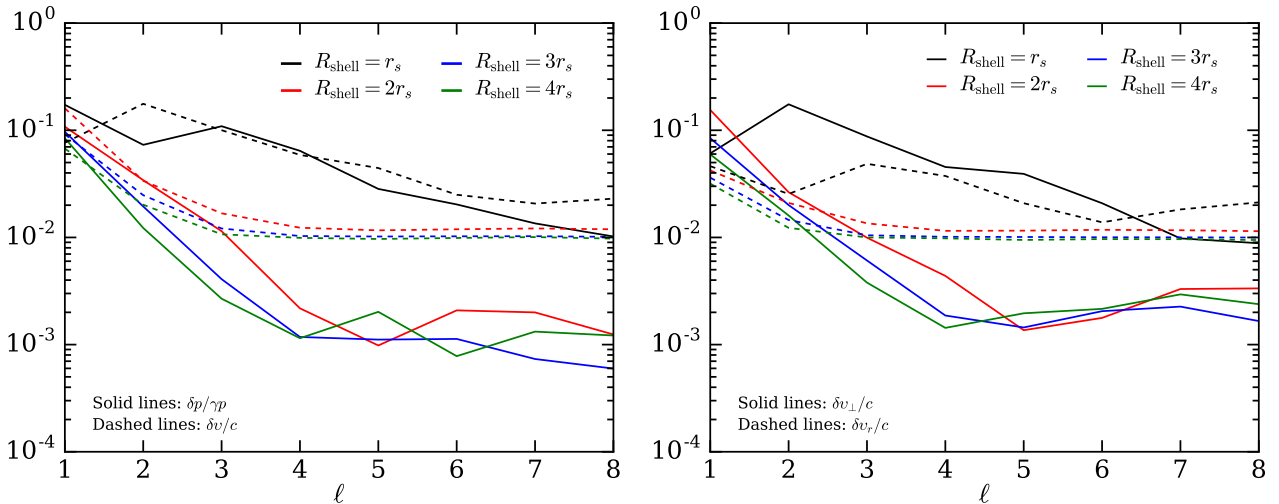


Figure 6. Left panel: Pressure (solid lines) and velocity (dashed lines) perturbations at $r = 0.1r_s$ generated by advected horizontal vorticity and horizontal vorticity as a function of angular wavenumber ℓ for different values of R_{shell} . The pressure perturbations are deduced from Eq. (A13), while velocity perturbations are deduced from Eqs. (A14) and (A10). **Right panel:** Transverse and radial velocity perturbations $\delta v_\perp/c$ (solid lines) and $\delta v_r/c$ (dashed lines) generated by advected horizontal vorticity waves as a function of ℓ for different values of R_{shell} at $r = 0.1r_s$.

large- R_{shell} waves have larger size and thus are more prone to radial stretching due to the acceleration of the flow. This results in weaker velocity and pressure perturbations in the inner regions of the flow. The velocity perturbations $\delta v/c$ are comparable to $\delta p/\gamma p$ for $\ell \leq 3$, as shown on the left panel of Fig. 6. For larger ℓ , velocity perturbations $\delta v/c$ are much larger than pressure variations $\delta p/\gamma p$. This is because, for larger ℓ , the generation of acoustic waves is not as efficient, so the velocity field is dominated by the contribution of the advected horizontal vorticity waves. The radial and tangential components of the velocity perturbations, shown on the left panel of Fig. 6, are comparable to each other for $\ell \lesssim 3$, but for larger ℓ , the radial component tends to dominate for most values of R_{shell} , which is expected for ra-

dially stretched vorticity waves. For reference, we provide the values of the amplitudes of the pressure and velocity perturbations at $r = 0.1r_s$ generated by advected entropy and horizontal vorticity waves in Table 1 for all of our perturbation parameters.

The radial profiles of the pressure and velocity perturbations generated by the advected entropy and horizontal vorticity perturbations are analyzed for different values of ℓ and R_{shell} in Fig. 7. The top three panels show the radial profile of $|\delta p/\gamma p|$ for $R_{\text{shell}} = r_s$, $R_{\text{shell}} = 2r_s$, and $R_{\text{shell}} = 3r_s$. The solid lines with different colors correspond to different values of ℓ ranging from 1 till 4. Similarly to the perturbations with $\ell = 2$ discussed above (cf. Fig 5), inside the sonic radius, $|\delta p/\gamma p|$ does not grow much with decreasing r .

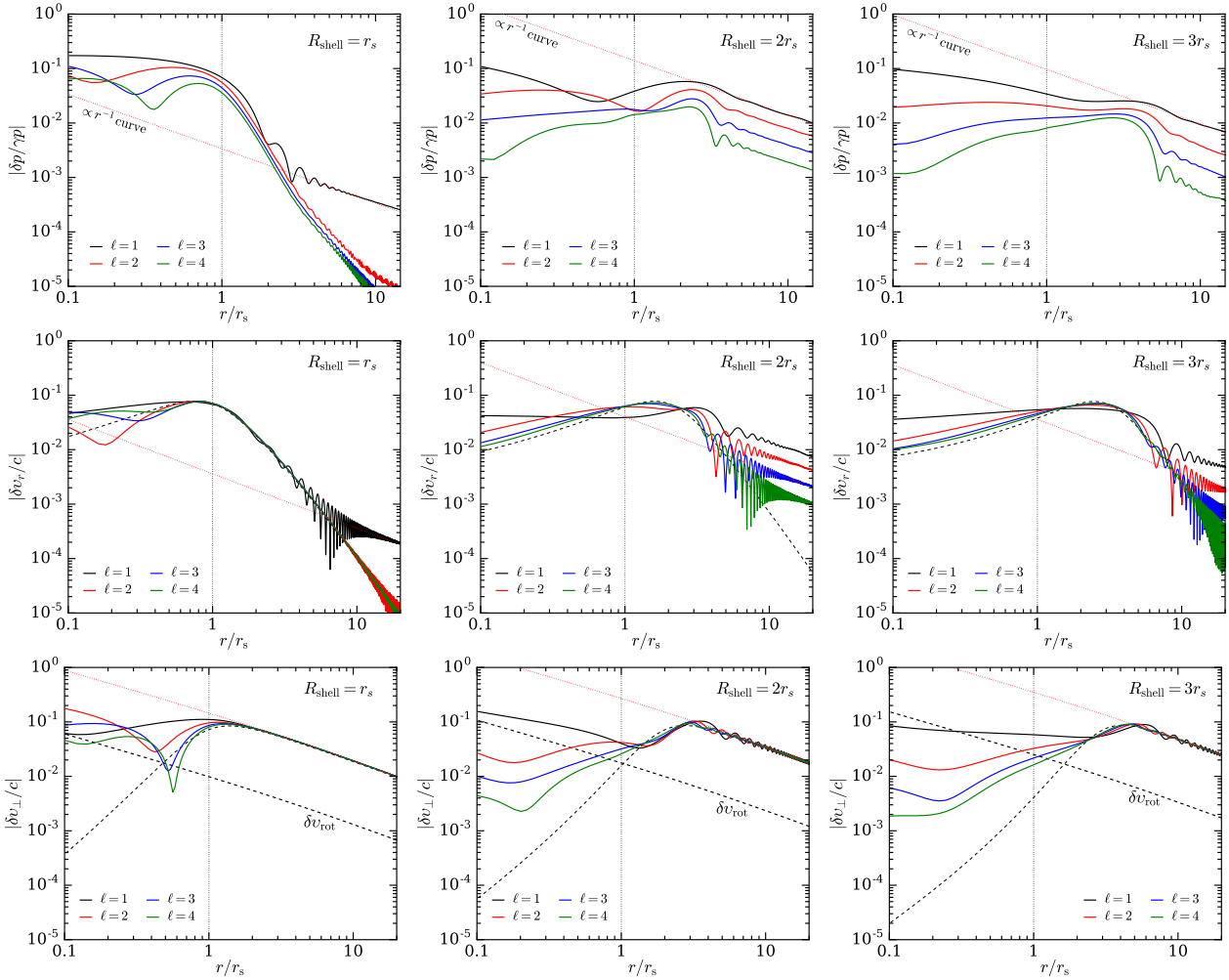


Figure 7. The top panels show the radial profile of the amplitude of $\delta p/\gamma p$ for acoustic waves generated by advected perturbations for different values of angular wavenumber ℓ and the initial radius of convective vortices R_{shell} , deduced from Eq. (A13). The amplitude $\delta p/\gamma p$ differs drastically at large radii for large R_{shell} , which is caused by the refraction of acoustic waves. Middle panels: Radial profile of $\delta v_r/c$ generated by advected horizontal vorticity waves for different values of ℓ and R_{shell} , deduced from Eq. (A10). Bottom panels: Radial profile of $\delta v_{\perp}/c$ generated by advected horizontal vorticity waves for different values of ℓ and R_{shell} , deduced from Eq. (A14). The dashed lines in the bottom six panels show the contribution of the advected horizontal vorticity waves only (i.e., the contribution of the acoustic waves are excluded), while the solid lines contain the contribution of both acoustic waves and advected horizontal vorticity waves. The straight red dotted lines in all panels show the $\propto r^{-1}$ slope for reference, while the dotted vertical line shows the location of the sonic point.

Instead, it exhibits a wave-like pattern with pressure perturbations varying by factor of ~ 2 . In the supersonic region, the overall value of $|\delta p/\gamma p|$ is consistent with the behavior at radius $0.1r_s$ that we saw in Fig. 6. At large radii $r > r_s$, $|\delta p/\gamma p|$ is stronger for perturbations with large R_{shell} (e.g., $R_{\text{shell}} \gtrsim 2r_s$). This is caused by the fact that, at large R_{shell} , perturbations have a large radial size, for which a significant fraction of incoming acoustic waves gets refracted back (Foglizzo 2001). These outgoing waves are identified owing to their $\propto r^{-1}$ scaling, which is a consequence of the conservation of energy. Since the amount of refraction decreases with the radial size, relatively little acoustic waves are present for, e.g., $R_{\text{shell}} = r_s$ at $r \gtrsim r_s$.

The radial profiles of $\delta v_r/c$ and $\delta v_{\perp}/c$ are shown in the bottom six panels of Fig. 7 for the same three values of R_{shell} . At large radii outside of the sonic point, both components of the velocity increase gradually with decreasing radius.

However, this increase saturates around the sonic point and almost no growth takes place in the supersonic region. This is again caused by the stretching of the vortex sheets due to the acceleration of the flow in the radial direction. We again see significantly more refracted acoustic waves at large radii for perturbations with larger R_{shell} . For outgoing waves, we observe the $\propto r^{-1}$ scaling which is again a consequence of the conservation of energy.

It is interesting to compare the total velocity perturbations (i.e., including the contributions of both acoustic and horizontal vorticity perturbations) to the velocity field of only horizontal vorticity waves (i.e., without including the contribution of acoustic waves) in the inner regions of the flow ($r \lesssim R_{\text{shell}}$). The former is shown with solid lines while the latter is shown with thin dashed lines in the six bottom panels of Fig. 7. The radial velocity acoustic waves is larger than that of horizontal vorticity waves by a factor

Table 1. The amplitudes of pressure and velocity perturbations generated by advected entropy and horizontal vorticity waves at radius $0.1r_s$, a radius where CCSN shock is expected to encounter the pre-collapse perturbations. The horizontal vorticity are normalized to yield a Mach number of 0.1 at the initial radius R_{shell} , while entropy fluctuations are assumed to have amplitude of $0.05 k_B/\text{baryon}$. The vertical component of vorticity scale as $\delta v_{\text{rot}}/c \sim 0.06(R_{\text{shell}}/r_s)^{0.9}$.

ℓ	R_{shell} [r_s]	$\frac{\delta p^{(v)}}{\gamma p}$ [10^{-2}]	$\frac{\delta v_r^{(v)}}{c}$ [10^{-2}]	$\frac{\delta v_{\perp}^{(v)}}{c}$ [10^{-2}]	$\frac{\delta p^{(e)}}{\gamma p}$ [10^{-2}]	$\frac{\delta v_r^{(e)}}{c}$ [10^{-2}]	$\frac{\delta v_{\perp}^{(e)}}{c}$ [10^{-2}]
1	1	17.3	4.54	5.74	0.92	0.85	2.01
1	2	10.8	4.17	15.4	0.49	0.68	0.84
1	3	9.64	3.45	8.22	0.59	1.06	1.89
1	4	8.34	2.91	5.48	1.20	1.28	2.33
2	1	7.19	2.47	17.5	1.32	0.62	0.70
2	2	3.39	1.86	2.53	0.45	0.97	0.77
2	3	1.87	1.01	1.90	0.53	1.04	0.64
2	4	1.08	0.59	1.51	0.57	1.08	0.53
3	1	10.9	4.83	8.73	0.67	0.54	0.76
3	2	1.12	1.01	0.94	0.21	0.90	0.33
3	3	0.34	0.45	0.56	0.23	0.95	0.25
3	4	0.16	0.27	0.31	0.21	0.96	0.22
4	1	6.41	3.67	4.48	0.44	0.77	0.78
4	2	0.16	0.74	0.39	0.15	0.88	0.20
4	3	0.02	0.44	0.08	0.12	0.91	0.17
4	4	0.02	0.31	0.05	0.11	0.93	0.13
5	1	2.80	1.90	3.89	0.43	0.87	0.48
5	2	0.06	0.77	0.04	0.08	0.86	0.13
5	3	0.10	0.48	0.03	0.04	0.89	0.14
5	4	0.19	0.36	0.08	0.08	0.88	0.18
6	1	2.01	1.12	2.08	0.31	0.81	0.19
6	2	0.21	0.84	0.11	0.03	0.83	0.14
6	3	0.11	0.48	0.09	0.03	0.88	0.19
6	4	0.05	0.31	0.08	0.06	0.91	0.20
7	1	1.33	1.68	0.97	0.24	0.70	0.12
7	2	0.19	0.81	0.24	0.06	0.84	0.23
7	3	0.04	0.45	0.12	0.06	0.89	0.19
7	4	0.09	0.31	0.15	0.10	0.91	0.26
8	1	1.00	2.01	0.82	0.22	0.68	0.33
8	2	0.08	0.75	0.25	0.09	0.86	0.22
8	3	0.04	0.45	0.07	0.05	0.89	0.15
8	4	0.10	0.33	0.12	0.07	0.89	0.21

^(v) Generated by advected vorticity waves.

^(e) Generated by advected entropy waves.

of a few. However, for $\delta v_{\perp}/c$, the contribution of acoustic waves exceed that of horizontal vorticity waves by a factor of $\sim 10^2$ for most perturbation parameters. Thus, the non-radial velocity perturbations ahead of the supernova shock is expected to be dominated by the contribution of acoustic waves. On the other hand, as discussed above, the velocity of the vertical vorticity δv_{rot} , shown with thick dashed lines in the bottom panels, grows as $\propto 1/r$. If it has an amplitude of 10^{-2} at the initial radius R_{shell} , which is 10 times smaller than that of the horizontal component, the contribution of the latter becomes significant. For $R_{\text{shell}} \geq 3r_s$, δv_{rot} becomes the dominant component of the velocity perturbations ahead of the CCSN shock.

4 CONCLUSION

In this work, we have studied the hydrodynamic evolution of convective perturbations in the nuclear-burning shells of massive stars during stellar collapse. The main aim was to investigate the physical properties of the perturbations when they reach the radius of ~ 150 km, where they are expected to encounter the supernova shock launched at core bounce. The properties of these perturbations affects the way they interact with the shock and thus influence the explosion dynamics. We modeled convection as a combination of vorticity and entropy waves and studied their evolution using linear hydrodynamics equations. Using the transonic Bondi solution to model the collapsing star, we followed the evolution of the hydrodynamic perturbations from large radii at a few $\sim 10^3$ km where they originate, down to small radii of ~ 150 km, where the flow is supersonic.

As the star collapses, vorticity and entropy perturbations move towards the center together with the stellar matter. Due to the converging geometry of the flow, the horizontal motions contract in the lateral direction, resulting in $\propto r^{-1}$ scaling of the velocity perturbations associated to the vertical vorticity. On the other hand, the velocities associated to the horizontal vorticity decrease with radius. This is caused by the acceleration of the collapse, which stretches the vortex sheets in the radial direction. In order to conserve the circulation, the velocity of vortex sheets has to decrease (cf. Section 3.2). The perturbations with large size are more prone to the radial stretching, leading to smaller velocity perturbations. As a result, ahead of the shock, the Mach number of vorticity waves do not exceed ~ 0.1 for most of the perturbation parameters.

Both entropy and horizontal vorticity perturbations, when advected with the flow, generate acoustic waves (cf. Section 3.3). This happens because, in converging flows, the advected perturbations do not remain in pressure equilibrium. The resulting pressure perturbations propagate as acoustic waves. We find that for models with $\ell = 1$ and $\ell = 2$, the pressure perturbations reach the relative amplitude of $\delta p/\gamma p \sim 0.1$ before encountering the supernova shock. This is in agreement with the results of 3D numerical simulations (Müller et al. 2017). The pressure perturbations are smaller for modes with larger ℓ . Due to the larger radial stretching by accelerated advection, convective vortices with large initial radii generate weak perturbations with a relative amplitude of $\sim 10^{-2}$ or smaller. We find that most of the radial velocity perturbations ahead of the CCSN shock consists of contributions from acoustic and, to a lesser extent, horizontal vorticity perturbations. The non-radial motion is dominated by the contributions from the acoustic waves as well as vertical vorticity perturbations.

Our present work sheds light on the physical properties of the perturbations ahead of the supernova shock. The interaction of vorticity, entropy, and acoustic waves with the shock can now be studied in more detail using, e.g., linear theory similar to that of Abdikamalov et al. (2018) with parameters appropriate for core-collapse supernovae. This will allow us to assess the relative importance of pre-shock acoustic, entropy, and vorticity perturbations on the post-shock dynamics. This will be the subject of a future work.

Finally, we point out that our work suffers from a number of limitations due to the simplifying assumptions that

we employ in our model. In particular, we use the stationary transonic Bondi solution to model the collapsing star. While this solution nicely captures the presence of subsonic and supersonic regions of accretion, in realistic stars, the dynamical collapse proceeds in a non-stationary fashion. Moreover, the real stars contain regions with different compositions and entropies. While these effects are incorporated in recent 3D simulations (e.g. Müller et al. 2017), the Bondi solution does not include them. In addition, the nuclear burning and neutrino cooling may still be taking place during the collapse phase. The adiabatic approximation that we use does not capture these effects. While these simplifications allowed us to obtain a unique insight into the evolution of the perturbations during collapse, the impact of these approximations needs to be carefully evaluated in future works.

ACKNOWLEDGEMENTS

The authors acknowledge fruitful discussions with César Huete, Ilya Kovalenko, Bernhard Müller, Jim Fuller, and Olzhas Mukazhanov. We also thank the anonymous referee for many constructive suggestions. The work was supported by Nazarbayev University Faculty Development Competitive Research Grant No. 090118FD5348, by the Ministry of Education of Kazakhstan’s target program IRN: BR05236454 and grant AP05135753. TF benefited from the KITP program on the “Mysteries and inner working of massive stars” supported by the National Science Foundation under Grant No. NSF PHY17-48958.

REFERENCES

- Abdikamalov E., Zhakysylykov A., Radice D., Berdibek S., 2016, *MNRAS*, **461**, 3864
- Abdikamalov E., Huete C., Nussupbekov A., Berdibek S., 2018, *Particles*, **1**, 7
- Bondi H., 1952, *MNRAS*, **112**, 195
- Buras R., Janka H.-T., Rampp M., Kifonidis K., 2006, *A&A*, **457**, 281
- Chandrasekhar S., 1961, *Hydrodynamic and Hydromagnetic Stability*. Clarendon, Oxford, UK
- Chatzopoulos E., Graziani C., Couch S. M., 2014, *ApJ*, **795**, 92
- Collins C., Müller B., Heger A., 2018, *MNRAS*, **473**, 1695
- Couch S. M., Ott C. D., 2013, *ApJ*, **778**, L7
- Couch S. M., Chatzopoulos E., Arnett W. D., Timmes F. X., 2015, *ApJ*, **808**, L21
- Foglizzo T., 2001, *A&A*, **368**, 311
- Foglizzo T., 2009, *ApJ*, **694**, 820
- Foglizzo T., Tagger M., 2000, *A&A*, **363**, 174
- Foglizzo T., Scheck L., Janka H.-T., 2006, *ApJ*, **652**, 1436
- Foglizzo T., Galletti P., Scheck L., Janka H.-T., 2007, *ApJ*, **654**, 1006
- Foglizzo T., et al., 2015, *Pub. Ast. Soc. Aus.*, **32**, e009
- Fuller J., 2017, *MNRAS*, **470**, 1642
- Fuller J., Cantiello M., Lecoanet D., Quataert E., 2015, *ApJ*, **810**, 101
- Goldreich P., Kumar P., 1990, *ApJ*, **363**, 694
- Huete C., Abdikamalov E., 2019, *Physica Scripta*, **94**, 094002
- Huete C., Abdikamalov E., Radice D., 2018, *MNRAS*, **475**, 3305
- Kazeroni R., Abdikamalov E., 2019, arXiv e-prints, p. [arXiv:1911.08819](https://arxiv.org/abs/1911.08819)
- Kippenhahn R., Weigert A., Weiss A., 2013, *Stellar Structure and Evolution*, doi:10.1007/978-3-642-30304-3.

- Kovalenko I. G., Eremin M. A., 1998, *MNRAS*, **298**, 861
- Kovaszny L. S. G., 1953, *Journal of the Aeronautical Sciences*, **20**, 657
- Lai D., Goldreich P., 2000, *ApJ*, **535**, 402
- Landau L. D., Lifshitz E. M., 1959, *Fluid Mechanics*, 2nd edition. Butterworth-Heinemann, Oxford, UK
- Lighthill M. J., 1952, *Proceedings of the Royal Society of London Series A*, **211**, 564
- Lighthill M. J., 1954, *Proceedings of the Royal Society of London A: Mathematical, Physical and Engineering Sciences*, **222**, 1
- Meakin C. A., Arnett D., 2007, *ApJ*, **665**, 690
- Müller B., 2016, *Publ. Astron. Soc. Australia*, **33**, e048
- Müller B., Janka H.-T., 2015, *MNRAS*, **448**, 2141
- Müller B., Viallet M., Heger A., Janka H.-T., 2016, *ApJ*, **833**, 124
- Müller B., Melson T., Heger A., Janka H.-T., 2017, *MNRAS*, **472**, 491
- Nagakura H., Takahashi K., Yamamoto Y., 2019, *MNRAS*, **483**, 208
- Quataert E., Shiode J., 2012, *MNRAS*, **423**, L92
- Radice D., Abdikamalov E., Ott C. D., Mösta P., Couch S. M., Roberts L. F., 2018, *Journal of Physics G Nuclear Physics*, **45**, 053003
- Takahashi K., Yamada S., 2014, *ApJ*, **794**, 162
- Takahashi K., Iwakami W., Yamamoto Y., Yamada S., 2016, *ApJ*, **831**, 75
- Thorne K. S., Blandford R. D., 2017, *Modern Classical Physics: Optics, Fluids, Plasmas, Elasticity, Relativity, and Statistical Physics*
- Yadav N., Bernhard Müller Janka H. T., Melson T., Heger A., 2019, arXiv e-prints, p. [arXiv:1905.04378](https://arxiv.org/abs/1905.04378)
- Yoshida T., Takiwaki T., Kotake K., Takahashi K., Nakamura K., Umeda H., 2019, arXiv e-prints, p. [arXiv:1903.07811](https://arxiv.org/abs/1903.07811)

APPENDIX A: LINEARIZED EQUATIONS FOR PERTURBATIONS

We start with the Euler equation,

$$\frac{\partial \mathbf{v}}{\partial t} + \boldsymbol{\omega} \times \mathbf{v} + \nabla \left(\frac{v^2}{2} + \frac{c^2}{\gamma - 1} - \frac{GM}{r} \right) = c^2 \nabla \frac{S}{\gamma}, \quad (\text{A1})$$

where $\boldsymbol{\omega} \equiv \nabla \times \mathbf{v}$ is the vorticity vector. The dimensionless entropy S is related to entropy per nucleon via equation $dS = ds_b/k_b$, where k_b is the Boltzmann constant (see Appendix E for the derivation). The equation for vorticity $\boldsymbol{\omega}$ can be obtained by combining the curl of Eq. (A1) with the continuity equation:

$$\frac{\partial}{\partial t} \frac{\boldsymbol{\omega}}{\rho} + (\mathbf{v} \cdot \nabla) \frac{\boldsymbol{\omega}}{\rho} = \left(\frac{\boldsymbol{\omega}}{\rho} \cdot \nabla \right) \mathbf{v} + \frac{1}{\rho} \nabla c^2 \times \nabla \frac{S}{\gamma} \quad (\text{A2})$$

The projection of the Euler equation along the direction of the flow yields an equation for the Bernoulli constant:

$$\left(\frac{\partial}{\partial t} + \mathbf{v} \cdot \nabla \right) \left(\frac{v^2}{2} + \frac{c^2}{\gamma - 1} - \frac{GM}{r} \right) = \frac{1}{\rho} \frac{\partial p}{\partial t}. \quad (\text{A3})$$

In the following, we separate the time dependence using the Fourier transform in time. We use the spherical coordinates (r, θ, ϕ) to describe the spatial dependence. The conservation of entropy during advection implies that

$$\delta S = \delta S_R e^{i\omega \int_R^r \frac{dr}{v}}, \quad (\text{A4})$$

while the conservation of δK yields

$$\delta K = \delta K_R e^{i\omega \int_R^r \frac{dr}{v}}, \quad (\text{A5})$$

where R is a coordinate where perturbations have zero phase and ω is the angular frequency. For clarity, we shall use a prime to distinguish the reference radius R' of the phase of advected perturbation in the supersonic region: $R > r_s$ and $R' < r_s$. The conservation laws of δK and δS across the sonic radius relate the solution defined for $R > r_s$ and the solution defined for $R' < r_s$:

$$\delta K_{R'} = \delta K_R e^{i\omega \int_R^{R'} \frac{dr}{v}}, \quad (\text{A6})$$

$$\delta S_{R'} = \delta S_R e^{i\omega \int_R^{R'} \frac{dr}{v}}. \quad (\text{A7})$$

Following [Foglizzo \(2001\)](#), we reformulate the linearized Euler equation using functions δf and δg :

$$\delta f \equiv v \delta v_r + \frac{2}{\gamma - 1} c \delta c, \quad (\text{A8})$$

$$\delta g \equiv \frac{\delta v_r}{v} + \frac{2}{\gamma - 1} \frac{\delta c}{c}. \quad (\text{A9})$$

The perturbations of the hydrodynamics quantities such as δv_r , δc , $\delta \rho$ and δp corresponding to δf and δg can be obtained by simply inverting relations (A8)-(A9) ([Foglizzo et al. 2007](#)):

$$\frac{\delta v_r}{v} = \frac{1}{1 - \mathcal{M}^2} \left(\delta g - \frac{\delta f}{c^2} \right), \quad (\text{A10})$$

$$\frac{\delta c^2}{c^2} = \frac{\gamma - 1}{1 - \mathcal{M}^2} \left(\frac{\delta f}{c^2} - \mathcal{M}^2 \delta g \right), \quad (\text{A11})$$

$$\frac{\delta \rho}{\rho} = \frac{1}{1 - \mathcal{M}^2} \left(-\mathcal{M}^2 \delta g - (1 - \mathcal{M}^2) \delta S + \frac{\delta f}{c^2} \right), \quad (\text{A12})$$

$$\frac{\delta p}{\gamma p} = \frac{1}{1 - \mathcal{M}^2} \left(-\mathcal{M}^2 \delta g - (1 - \mathcal{M}^2) \frac{\delta S}{\gamma} + \frac{\delta f}{c^2} \right). \quad (\text{A13})$$

The transverse velocity component can be expressed in terms of δf and δK (cf. Appendix D):

$$\delta v_\perp = \frac{1}{i\omega r} \left(\delta f - \frac{\delta K}{L^2} \right). \quad (\text{A14})$$

We can obtain a system of differential equations for δf and δg by combining the continuity equation with the radial projection of the Euler equation:

$$v \frac{\partial \delta f}{\partial r} + \frac{i\omega \mathcal{M}^2 \delta f}{1 - \mathcal{M}^2} = \frac{i\omega v^2 \delta g}{1 - \mathcal{M}^2} + i\omega c^2 \frac{\delta S_R}{\gamma} e^{i\omega \int_R^r \frac{dr}{v}}, \quad (\text{A15})$$

$$v \frac{\partial \delta g}{\partial r} + \frac{i\omega \mathcal{M}^2 \delta g}{1 - \mathcal{M}^2} = \frac{i\omega \delta f}{c^2(1 - \mathcal{M}^2)} + \frac{i}{\omega} \Delta_{\theta, \varphi} \delta f + \frac{i\delta K_R}{r^2 \omega} e^{i\omega \int_R^r \frac{dr}{v}}, \quad (\text{A16})$$

where $\Delta_{\theta, \varphi}$ is the angular part of the Laplacian. The homogeneous system associated with this system describes propagation of free acoustic waves. In the presence of inhomogeneous terms δK and δS , which model advected vorticity and entropy perturbations, the solution of this system has multiple components: the vorticity and entropy perturbations themselves as well as the acoustic waves that these two perturbations generate. The contribution of acoustic waves as well as vorticity and entropy waves to the values of δf and δg can be separated using the decomposition of [Foglizzo et al. \(2007\)](#), as described in Appendix F. Using the spherical har-

monics $Y_l^m(\theta, \varphi)$ decomposition, we obtain:

$$v \frac{\partial \delta f}{\partial r} + \frac{i\omega \mathcal{M}^2 \delta f}{1 - \mathcal{M}^2} = \frac{i\omega v^2 \delta g}{1 - \mathcal{M}^2} + i\omega c^2 \frac{\delta S_R}{\gamma} e^{i\omega \int_R^r \frac{dr}{v}}, \quad (\text{A17})$$

$$v \frac{\partial \delta g}{\partial r} + \frac{i\omega \mathcal{M}^2 \delta g}{1 - \mathcal{M}^2} = \frac{i\omega \delta f}{c^2(1 - \mathcal{M}^2)} - \frac{iL^2}{\omega r^2} \delta f + \frac{i\delta K_R}{r^2 \omega} e^{i\omega \int_R^r \frac{dr}{v}}. \quad (\text{A18})$$

In either region $r > r_s$ or $r < r_s$, we define quantities $\delta \tilde{f}$ and $\delta \tilde{g}$ as:

$$\delta \tilde{f} \equiv e^{i\omega \int_R^r \frac{\mathcal{M}^2}{1 - \mathcal{M}^2} \frac{dr}{v}} \delta f, \quad (\text{A19})$$

$$\delta \tilde{g} \equiv e^{i\omega \int_R^r \frac{\mathcal{M}^2}{1 - \mathcal{M}^2} \frac{dr}{v}} \delta g. \quad (\text{A20})$$

where the lower bound R of the integral is chosen in the same region. Despite the mathematical singularity at $r = r_s$, the differential system deduced from equations (A17)-(A18) in each half domain $r > r_s$ or $r < r_s$ is formally simpler:

$$\frac{\partial \delta \tilde{f}}{\partial r} = \frac{i\omega v \delta \tilde{g}}{1 - \mathcal{M}^2} + i\omega \frac{c^2}{v} \frac{\delta S_R}{\gamma} e^{i\omega \int_R^r \frac{dr}{v(1 - \mathcal{M}^2)}}, \quad (\text{A21})$$

$$\frac{\partial \delta \tilde{g}}{\partial r} = \frac{i\delta \tilde{f}}{\omega v} \left[\frac{\omega^2}{c^2(1 - \mathcal{M}^2)} - \frac{L^2}{r^2} \right] + \frac{i\delta K_R}{r^2 \omega v} e^{i\omega \int_R^r \frac{dr}{v(1 - \mathcal{M}^2)}} \quad (\text{A22})$$

Using the new variable X , which is related to r via equation

$$\frac{dX}{dr} \equiv \frac{v}{1 - \mathcal{M}^2}, \quad (\text{A23})$$

system (A21)-(A22) can be combined into a more compact form:

$$\frac{\partial^2 \delta \tilde{f}}{\partial X^2} + W \tilde{f} = -\frac{1 - \mathcal{M}^2}{v} e^{i\omega \int_R^r \frac{dr}{v}} \times \left\{ \frac{\omega}{\mathcal{M}^2} \frac{\delta S_R}{\gamma} \left(\frac{\omega}{v} + i \frac{\partial \log \mathcal{M}^2}{\partial r} \right) + \frac{\delta K_R}{v r^2} \right\}, \quad (\text{A24})$$

where

$$W \equiv \frac{1}{v^2 c^2} (\omega^2 - \omega_l^2). \quad (\text{A25})$$

and

$$\omega_l^2 \equiv l(l+1) \frac{c^2 - v^2}{r^2}. \quad (\text{A26})$$

APPENDIX B: APPROXIMATE SOLUTIONS OF THE HOMOGENEOUS EQUATION

B1 WKB approximation at large radii

The general solution of the homogeneous equation,

$$\frac{\partial^2 \delta \tilde{f}}{\partial X^2} + W \delta \tilde{f} = 0, \quad (\text{B1})$$

associated with equation (A24) is a linear combination of outgoing (δf^-) and ingoing (δf^+) acoustic waves. At the outer boundary, we obtain these two using the WKB approximation ([Foglizzo 2001](#)):

$$\delta \tilde{f}^\pm \sim A_\pm \frac{\omega^{\frac{1}{2}}}{W^{\frac{1}{4}}} e^{i\omega \int_R^\infty \frac{\mathcal{M}^2}{1 - \mathcal{M}^2} \frac{dr}{v}} \exp \left(\pm i \int^r \frac{v W^{\frac{1}{2}}}{1 - \mathcal{M}^2} dr \right), \quad (\text{B2})$$

$$\delta f^\pm \sim A_\pm \frac{\omega^{\frac{1}{2}}}{W^{\frac{1}{4}}} \exp \left(i\omega \int_r^\infty \frac{\mathcal{M}^2}{1 - \mathcal{M}^2} \frac{dr}{v} \pm i \int^r \frac{v W^{\frac{1}{2}}}{1 - \mathcal{M}^2} dr \right), \quad (\text{B3})$$

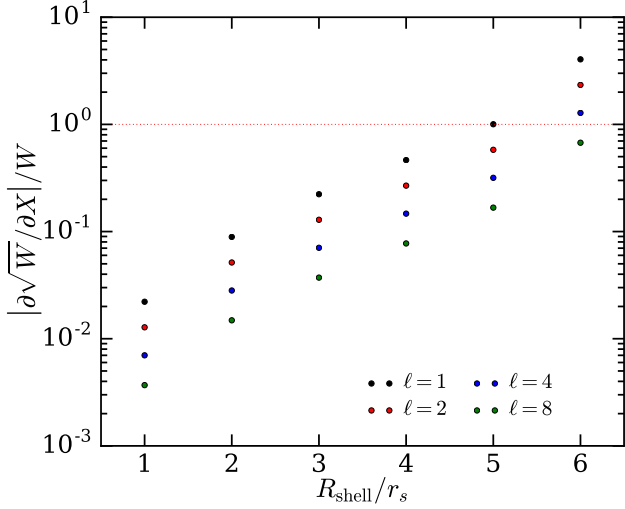


Figure B1. Ratio $|\partial\sqrt{W}/\partial X|/W$, which measures the degree of the validity of the WKB approximation, as a function of initial radius of the vortices for different values of ℓ at radius $r = 40r_s$.

where A_{\pm} is a complex amplitude such that $|A_-| = |A_+|$ is homogeneous to a velocity. The WKB approximation is satisfied at large radii from the center or for high-frequency perturbations. These two conditions are consistent with the requirement that

$$\left| \frac{\partial\sqrt{W}}{\partial X} \right| \ll W, \quad (\text{B4})$$

Figure B1 shows the ratio $|\partial\sqrt{W}/\partial X|/W$, which measures the degree of the validity of the WKB approximation, as a function of initial radius of the vortices R_{shell} for different values of ℓ at the outer boundary of our computational domain. The latter is chosen to be at $r = 40r_s$ for our setup. As we can see the ratio is below 1 for $R_{\text{shell}} < 5r_s$. For this reason, we consider initial radii ranging from r_s to $4r_s$, where WKB is expected to yield accurate result.

The Wronskien \mathcal{W} of $\delta\tilde{f}^+$ and $\delta\tilde{f}^-$ (or the pair of solutions $\delta\tilde{f}_0$ and $\delta\tilde{f}^-$), on either side of the sonic point, is:

$$\mathcal{W} \equiv \tilde{f}^+ \frac{\partial\tilde{f}^-}{\partial r} - \tilde{f}^- \frac{\partial\tilde{f}^+}{\partial r} = -\frac{2i\omega v}{1 - \mathcal{M}^2} A_R, \quad (\text{B5})$$

$$A_R \equiv A_+ A_- e^{2i\omega \int_R^\infty \frac{\mathcal{M}^2}{1 - \mathcal{M}^2} \frac{dr}{v}}. \quad (\text{B6})$$

The Wronskien of $(\delta f_0, \delta f^-)$ or $(\delta f^+, \delta f^-)$ is independent of the boundary R :

$$\delta f_0 \frac{\partial\delta f^-}{\partial r} - \delta f^- \frac{\partial\delta f_0}{\partial r} = -\frac{2i\omega v}{1 - \mathcal{M}^2} A_+ A_- e^{-2i\omega \int_R^\infty \frac{\mathcal{M}^2}{1 - \mathcal{M}^2} \frac{dr}{v}}. \quad (\text{B7})$$

We note that $\delta\tilde{f}_0$ is singular at the sonic point. On either side of the sonic radius,

$$\delta\tilde{f}^- \delta\tilde{g}_0 - \delta\tilde{f}_0 \delta\tilde{g}^- = 2A_R, \quad (\text{B8})$$

$$\delta f^- \delta g_0 - \delta f_0 \delta g^- = 2A_+ A_- e^{-2i\omega \int_\infty^R \frac{\mathcal{M}^2}{1 - \mathcal{M}^2} \frac{dr}{v}}. \quad (\text{B9})$$

B2 Approximation in the supersonic region

At high Mach number the velocity approaches free fall and the sound speed is deduced from mass conservation of the isentropic gas:

$$v \propto r^{-\frac{1}{2}}, \quad (\text{B10})$$

$$c \propto \left(\frac{1}{vr^2} \right)^{\frac{\gamma-1}{2}} \sim r^{-\frac{3}{4}(\gamma-1)}, \quad (\text{B11})$$

$$\mathcal{M} \propto r^{\frac{3}{4}(\gamma-1) - \frac{1}{2}} \quad (\text{B12})$$

The phase relation between δf and $\delta\tilde{f}$ is thus a converging function when $r \rightarrow 0$. According to the differential system (A24),

$$\frac{\partial^2 \delta f}{\partial r^2} \propto \frac{\delta f}{r^2 c^2} \propto \delta f r^{-\frac{3}{2}} \quad (\text{B13})$$

It implies that the homogeneous solution δf is bounded when $r \rightarrow 0$.

$$\delta f \propto e^{r^{\frac{1}{2}}} \quad (\text{B14})$$

APPENDIX C: SOLUTIONS WITH ENTROPY AND VORTICITY PERTURBATIONS

C1 Solution for vorticity perturbations

The solution of equation (A24) for the case with $\delta K \neq 0$ and $\delta S = 0$ can be obtained using the method of variation of parameters. The two free parameters of the method are fixed by (1) imposing the regularity at $r = r_s$ and (2) assuming that no sound waves come from infinity, which leads to the solution (Foglizzo 2001)

$$\begin{aligned} \delta f(r > r_s) &= -\frac{i\delta K_R}{2\omega A_R} \\ &\times \left\{ \delta f^- \int_{r_s}^r e^{i\omega \int_R^r \frac{1+\mathcal{M}^2}{1-\mathcal{M}^2} \frac{dr}{v}} \frac{\delta f_0}{r^2 v} dr \right. \\ &\left. - \delta f_0 \int_{\infty}^r e^{i\omega \int_R^r \frac{1+\mathcal{M}^2}{1-\mathcal{M}^2} \frac{dr}{v}} \frac{\delta f^-}{r^2 v} dr \right\}, \quad (\text{C1}) \end{aligned}$$

where $R > r_s$, δf_0 is the regular homogeneous solution. δf^- corresponds to outgoing acoustic waves when $r \gg r_s$, normalized according to Eq. (B2). The function δf^- is singular at the sonic radius. The Wronskien associated to the pair $(\delta f_0, \delta f^-)$ satisfies Eq. (B5).

As in Foglizzo (2001), an integration by part is used to accelerate the convergence as r^{-5} at infinity

$$\begin{aligned} \delta f(r > r_s) &= \frac{\delta K_R}{2\omega^2 A_R} \times \\ &\left\{ \delta f^- \int_{r_s}^r e^{i\omega \int_R^r \frac{1+\mathcal{M}^2}{1-\mathcal{M}^2} \frac{dr}{v}} \left[\frac{\partial}{\partial r} \left(\frac{1 - \mathcal{M}^2}{r^2} \right) \delta f_0 + \frac{i\omega v}{r^2} \delta g_0 \right] dr \right. \\ &\left. - \delta f_0 \int_{\infty}^r e^{i\omega \int_R^r \frac{1+\mathcal{M}^2}{1-\mathcal{M}^2} \frac{dr}{v}} \left[\frac{\partial}{\partial r} \left(\frac{1 - \mathcal{M}^2}{r^2} \right) \delta f^- + \frac{i\omega v}{r^2} g^- \right] dr \right\}, \quad (\text{C2}) \end{aligned}$$

We use the regular solution δf_0 and the technique of variation of constants to define a second solution δf_{sup} of the

homogeneous equation in the supersonic region:

$$\begin{aligned} \delta f_{\text{sup}}(r < r_s) &\equiv -2i\omega A_R \delta f_0 \\ &\times \int_{R'}^r e^{-2i\omega \int_{R'}^r \frac{M^2}{1-M^2} \frac{dr}{v}} \frac{v}{\delta f_0^2} \frac{dr}{1-M^2}, \end{aligned} \quad (\text{C3})$$

It is singular at the sonic point. The singularity of the integral is isolated using an integration by parts:

$$\begin{aligned} \delta f_{\text{sup}}(r) &= A_R \delta f_0 \left\{ \left[e^{-2i\omega \int_{R'}^r \frac{M^2}{1-M^2} \frac{dr}{v}} \frac{c^2}{\delta f_0^2} \right]_{R'}^r \right. \\ &\quad \left. - \int_{R'}^r e^{-2i\omega \int_{R'}^r \frac{M^2}{1-M^2} \frac{dr}{v}} \frac{\partial}{\partial r} \left(\frac{c^2}{\delta f_0^2} \right) dr \right\}, \\ &= A_R \delta f_0 \left\{ \left[e^{-2i\omega \int_{R'}^r \frac{M^2}{1-M^2} \frac{dr}{v}} \frac{c^2}{\delta f_0^2} \right]_{R'}^r \right. \\ &\quad \left. - \int_{R'}^r e^{-2i\omega \int_{R'}^r \frac{M^2}{1-M^2} \frac{dr}{v}} \right. \\ &\quad \left. \times \frac{1}{\delta f_0^3} \left(\delta f_0 \frac{\partial c^2}{\partial r} - 2c^2 \frac{\partial \delta f_0}{\partial r} \right) dr \right\}. \end{aligned} \quad (\text{C4})$$

The singular phase is also calculated using an integration by parts:

$$\begin{aligned} \int_{R'}^r \frac{1+M^2}{1-M^2} \frac{dr}{v} &= \left[\frac{1+M^2}{v} \frac{r-r_s}{1-M^2} \log|r-r_s| \right]_{R'}^r \\ &\quad - \int_{R'}^r \log|r-r_s| \frac{\partial}{\partial r} \left(\frac{1+M^2}{v} \frac{r-r_s}{1-M^2} \right) dr, \end{aligned} \quad (\text{C5})$$

or

$$\begin{aligned} \int_{R'}^r \frac{1+M^2}{1-M^2} \frac{dr}{v} &= \\ &= \left[\frac{1+M^2}{v} \left(\frac{\partial M^2}{\partial r} \right)^{-1} \log|1-M^2| \right]_{R'}^r \\ &\quad + \int_{R'}^r \log|1-M^2| \frac{\partial}{\partial r} \left[\frac{1+M^2}{v} \left(\frac{\partial M^2}{\partial r} \right)^{-1} \right] dr. \end{aligned} \quad (\text{C6})$$

In derivation of the last equations, we have used the radial derivated of the Mach number:

$$\frac{\partial M^2}{\partial r} = 2(\gamma-1) \frac{M^2}{r} - \frac{\gamma+1}{1-M^2} \left(2 - \frac{1}{rc^2} \right) \frac{M^2}{r}, \quad (\text{C7})$$

and

$$\begin{aligned} \frac{\partial^2 M^2}{\partial r^2} &= -2(\gamma-1) \frac{M^2}{r^2} + 2 \frac{\gamma-1}{r} \frac{\partial M^2}{\partial r} \\ &\quad - \frac{\gamma+1}{(1-M^2)^2} \left(\frac{2}{r} - \frac{1}{r^2 c^2} \right) \frac{\partial M^2}{\partial r} \\ &\quad + \frac{\gamma+1}{r^2} \frac{2M^2}{1-M^2} \left[1 - \frac{1}{c^2} \left(\frac{1}{r} + \frac{\partial \log c}{\partial r} \right) \right]. \end{aligned} \quad (\text{C8})$$

The definition of the function δg_{sup} follows from Eq. (A22):

$$\delta g_{\text{sup}}(r < r_s) \equiv \frac{1}{\delta f_0} \left(\delta g_0 \delta f_{\text{sup}} - 2A_R e^{-2i\omega \int_{R'}^r \frac{M^2}{1-M^2} \frac{dr}{v}} \right). \quad (\text{C9})$$

The normalization factor $(-2i\omega A_R)$ in Eq. (C3) has been chosen so that the Wronskien of $(\delta f_0, \delta f_{\text{sup}})$ is the same as

$(\delta f_0, \delta f^-)$ as defined by Eq. (B5). We define a general solution in the supersonic part of the flow which is regular at the sonic point and matches the subsonic solution given by Eq. (C1) at $r = r_s$:

$$\begin{aligned} \delta f(r < r_s) &= -\frac{i\delta K_{R'}}{2\omega A_R} \times \\ &\quad \left\{ \delta f_{\text{sup}} \int_{r_s}^r \frac{\delta f_0}{r^2 v} e^{i\omega \int_{R'}^r \frac{1+M^2}{1-M^2} \frac{dr}{v}} dr \right. \\ &\quad \left. - \delta f_0 \int_{r_s}^r \frac{\delta f_{\text{sup}}}{r^2 v} e^{i\omega \int_{R'}^r \frac{1+M^2}{1-M^2} \frac{dr}{v}} dr \right. \\ &\quad \left. - \delta f_0 e^{i\omega \int_{R'}^r \frac{dr}{v}} \int_{\infty}^{r_s} \frac{\delta f^-}{r^2 v} e^{i\omega \int_{R'}^r \frac{1+M^2}{1-M^2} \frac{dr}{v}} dr \right\}. \end{aligned} \quad (\text{C10})$$

A faster convergence near the origin is obtained by using an integration by parts:

$$\begin{aligned} &\int_{r_s}^r e^{i\omega \int_{R'}^r \frac{1+M^2}{1-M^2} \frac{dr}{v}} \frac{\delta f_0}{r^2 v} dr \\ &= \int_{r_s}^r e^{i\omega \int_{R'}^r \frac{1}{1-M^2} \frac{dr}{v}} \frac{i\omega}{L^2 + \frac{\omega^2 r^2}{v^2 - c^2}} \frac{\partial \delta \tilde{g}_0}{\partial r} dr \\ &= \left[e^{i\omega \int_{R'}^r \frac{1}{1-M^2} \frac{dr}{v}} \frac{i\omega}{L^2 + \frac{\omega^2 r^2}{v^2 - c^2}} \delta \tilde{g}_0 \right]_{r_s}^r \\ &\quad - \int_{r_s}^r \delta \tilde{g}_0 \frac{\partial}{\partial r} \left(e^{i\omega \int_{R'}^r \frac{1}{1-M^2} \frac{dr}{v}} \frac{i\omega}{L^2 + \frac{\omega^2 r^2}{v^2 - c^2}} \right) dr. \end{aligned} \quad (\text{C11})$$

In consequence, each integral is now convergent when $r \rightarrow 0$:

$$\begin{aligned} &\delta f_{\text{sup}} \int_{r_s}^r \frac{\delta \tilde{f}_0}{r^2 v} e^{i\omega \int_{R'}^r \frac{dr}{v(1-M^2)}} dr \\ &\quad - \delta f_0 \int_{r_s}^r \frac{\delta \tilde{f}_{\text{sup}}}{r^2 v} e^{i\omega \int_{R'}^r \frac{dr}{v(1-M^2)}} dr = e^{i\omega \int_{R'}^r \frac{dr}{v}} \frac{2i\omega A_R}{L^2 + \frac{\omega^2 r^2}{v^2 - c^2}} \\ &\quad - \delta f_{\text{sup}} \int_{r_s}^r \delta \tilde{g}_0 \frac{\partial}{\partial r} \left(e^{i\omega \int_{R'}^r \frac{1}{1-M^2} \frac{dr}{v}} \frac{i\omega}{L^2 + \frac{\omega^2 r^2}{v^2 - c^2}} \right) dr \\ &\quad + \delta f_0 \int_{r_s}^r \delta \tilde{g}_{\text{sup}} \frac{\partial}{\partial r} \left(e^{i\omega \int_{R'}^r \frac{1}{1-M^2} \frac{dr}{v}} \frac{i\omega}{L^2 + \frac{\omega^2 r^2}{v^2 - c^2}} \right) dr. \end{aligned} \quad (\text{C12})$$

Note that, in deriving the last equation, we used the relation $\delta \tilde{f}_{\text{sup}} \delta \tilde{g}_0 - \delta \tilde{f}_0 \delta \tilde{g}_{\text{sup}} = 2A_R$. Using equation (A21), we can rewrite this relation as

$$\begin{aligned} &\delta f_{\text{sup}} \int_{r_s}^r \frac{\delta \tilde{f}_0}{r^2 v} e^{i\omega \int_{R'}^r \frac{dr}{v(1-M^2)}} dr \\ &\quad - \delta f_0 \int_{r_s}^r \frac{\delta \tilde{f}_{\text{sup}}}{r^2 v} e^{i\omega \int_{R'}^r \frac{dr}{v(1-M^2)}} dr = e^{i\omega \int_{R'}^r \frac{dr}{v}} \frac{2i\omega A_R}{L^2 + \frac{\omega^2 r^2}{v^2 - c^2}} \\ &\quad - \delta f_{\text{sup}} \int_{r_s}^r \frac{1-M^2}{v} \frac{\partial \delta \tilde{f}_0}{\partial r} \frac{\partial}{\partial r} \left(e^{i\omega \int_{R'}^r \frac{1}{1-M^2} \frac{dr}{v}} \frac{i\omega}{L^2 + \frac{\omega^2 r^2}{v^2 - c^2}} \right) dr \\ &\quad + \delta f_0 \int_{r_s}^r \frac{1-M^2}{v} \frac{\partial \delta \tilde{f}_{\text{sup}}}{\partial r} \frac{\partial}{\partial r} \left(e^{i\omega \int_{R'}^r \frac{1}{1-M^2} \frac{dr}{v}} \frac{i\omega}{L^2 + \frac{\omega^2 r^2}{v^2 - c^2}} \right) dr, \end{aligned}$$

thus

$$\begin{aligned} & \delta f_{\text{sup}} \int_{r_s}^r \frac{\delta \tilde{f}_0}{r^2 v} e^{i\omega \int_{R'}^r \frac{dr}{v(1-M^2)}} dr \\ & - \delta f_0 \int_{r_s}^r \frac{\delta \tilde{f}_{\text{sup}}}{r^2 v} e^{i\omega \int_{R'}^r \frac{dr}{v(1-M^2)}} dr = e^{i\omega \int_{R'}^r \frac{dr}{v}} \frac{2i\omega A_R}{L^2 + \frac{\omega^2 r^2}{v^2 - c^2}} \\ & + \delta f_{\text{sup}} \int_{r_s}^r \delta \tilde{f}_0 \frac{\partial}{\partial r} \left[\frac{1-M^2}{v} \frac{\partial}{\partial r} \left(\frac{e^{i\omega \int_{R'}^r \frac{1}{1-M^2} \frac{dr}{v}}}{L^2 + \frac{\omega^2 r^2}{v^2 - c^2}} \right) \right] dr \\ & - \delta f_0 \int_{r_s}^r \delta \tilde{f}_{\text{sup}} \frac{\partial}{\partial r} \left[\frac{1-M^2}{v} \frac{\partial}{\partial r} \left(\frac{e^{i\omega \int_{R'}^r \frac{1}{1-M^2} \frac{dr}{v}}}{L^2 + \frac{\omega^2 r^2}{v^2 - c^2}} \right) \right] dr. \end{aligned} \quad (\text{C13})$$

C2 Acoustic field of entropy perturbations

The general solution for the advected entropy waves can be obtained by linearly superposing the solution for $\delta K = L^2 \delta S / \gamma$, which accounts for the contribution of the vorticity generated by the advected entropy waves, with the solution for $\delta S \neq 0$ and $\delta K = 0$. The latter can be written as follows, provided that it is regular at the sonic point and provided that there are no acoustic waves coming from infinity (Foglizzo 2001),

$$\begin{aligned} \delta f(r > r_s) &= -\frac{\delta S_R}{2\gamma A_R} \\ & \times \left\{ \delta f^- \int_{r_s}^r \delta \tilde{f}_0 \frac{\partial}{\partial r} \left(\frac{1-M^2}{M^2} e^{i\omega \int_{R'}^r \frac{dr}{v(1-M^2)}} \right) dr \right. \\ & \left. - \delta f_0 \int_{\infty}^r \delta \tilde{f}^- \frac{\partial}{\partial r} \left(\frac{1-M^2}{M^2} e^{i\omega \int_{R'}^r \frac{dr}{v(1-M^2)}} \right) dr \right\}, \end{aligned} \quad (\text{C14})$$

After an integration by parts the integrated terms cancel out:

$$\begin{aligned} \delta f(r > r_s) &= \frac{\delta S_R}{2\gamma A_R} \\ & \times \left\{ \delta f^- \int_{r_s}^r \frac{\partial \delta \tilde{f}_0}{\partial r} \left(\frac{1-M^2}{M^2} e^{i\omega \int_{R'}^r \frac{dr}{v(1-M^2)}} \right) dr \right. \\ & \left. - \delta f_0 \int_{\infty}^r \frac{\partial \delta \tilde{f}^-}{\partial r} \left(\frac{1-M^2}{M^2} e^{i\omega \int_{R'}^r \frac{dr}{v(1-M^2)}} \right) dr \right\}. \end{aligned} \quad (\text{C15})$$

After a second integration by parts, the integrals converge at infinity:

$$\begin{aligned} \delta f(r > r_s) &= -\frac{\delta S_R}{2\gamma i\omega A_R} \\ & \times \left\{ -\frac{v(1-M^2)^2}{M^2} \left(\delta f^- \frac{\partial \delta \tilde{f}_0}{\partial r} - \delta f_0 \frac{\partial \delta \tilde{f}^-}{\partial r} \right) e^{i\omega \int_{R'}^r \frac{dr}{v(1-M^2)}} \right. \\ & + \delta f^- \int_{r_s}^r \frac{\partial}{\partial r} \left[\frac{v(1-M^2)^2}{M^2} \frac{\partial \delta \tilde{f}_0}{\partial r} \right] e^{i\omega \int_{R'}^r \frac{dr}{v(1-M^2)}} dr \\ & \left. - \delta f_0 \int_{\infty}^r \frac{\partial}{\partial r} \left[\frac{v(1-M^2)^2}{M^2} \frac{\partial \delta \tilde{f}^-}{\partial r} \right] e^{i\omega \int_{R'}^r \frac{dr}{v(1-M^2)}} dr \right\}, \end{aligned}$$

thus

$$\begin{aligned} \delta f(r > r_s) &= \frac{\delta S_R}{\gamma} (c^2 - v^2) e^{i\omega \int_{R'}^r \frac{dr}{v}} - \frac{\delta S_R}{2\gamma i\omega A_R} \\ & \times \left\{ \delta f^- \int_{r_s}^r \frac{\partial}{\partial r} \left[\frac{v(1-M^2)^2}{M^2} \frac{\partial \delta \tilde{f}_0}{\partial r} \right] e^{i\omega \int_{R'}^r \frac{dr}{v(1-M^2)}} dr \right. \\ & \left. - \delta f_0 \int_{\infty}^r \frac{\partial}{\partial r} \left[\frac{v(1-M^2)^2}{M^2} \frac{\partial \delta \tilde{f}^-}{\partial r} \right] e^{i\omega \int_{R'}^r \frac{dr}{v(1-M^2)}} dr \right\}, \end{aligned}$$

or

$$\begin{aligned} \delta f(r > r_s) &= \frac{\delta S_R}{\gamma} (c^2 - v^2) e^{i\omega \int_{R'}^r \frac{dr}{v}} \\ & - \frac{\delta S_R}{2\gamma A_R} \left\{ \delta f^- \int_{r_s}^r \frac{\partial}{\partial r} \left[(c^2 - v^2) \delta \tilde{g}_0 \right] e^{i\omega \int_{R'}^r \frac{dr}{v(1-M^2)}} dr \right. \\ & \left. - \delta f_0 \int_{\infty}^r \frac{\partial}{\partial r} \left[(c^2 - v^2) \delta \tilde{g}^- \right] e^{i\omega \int_{R'}^r \frac{dr}{v(1-M^2)}} dr \right\}, \end{aligned} \quad (\text{C16})$$

The functions $A_k(r), B_k(r)$ are obtained by integrating by parts:

$$\begin{aligned} \delta f(r > r_s) &= \frac{\delta S_R}{\gamma} D_k e^{i\omega \int_{R'}^r \frac{dr}{v}} \\ & + \frac{\delta S_R}{2\gamma A_R} \left\{ \delta f^- \int_{r_s}^r e^{i\omega \int_{R'}^r \frac{1+M^2}{1-M^2} \frac{dr}{v}} (A_k \delta f_0 + B_k \delta g_0) dr \right. \\ & \left. - \delta f_0 \int_{\infty}^r e^{i\omega \int_{R'}^r \frac{1+M^2}{1-M^2} \frac{dr}{v}} (A_k \delta f^- + B_k \delta g^-) dr \right\}, \end{aligned} \quad (\text{C17})$$

with

$$A_1 \equiv -\frac{i\omega}{v} \left(1 - \frac{\omega_L^2}{\omega^2} \right) \propto r^2, \quad (\text{C18})$$

$$B_1 \equiv -\frac{\partial}{\partial r} (c^2 - v^2) \propto r^{-2}, \quad (\text{C19})$$

$$D_1 \equiv c^2 - v^2 \quad (\text{C20})$$

After an integration by parts

$$\begin{aligned} \delta f(r > r_s) &= \frac{\delta S_R}{\gamma} e^{i\omega \int_{R'}^r \frac{dr}{v}} \\ & \times \left[D_k + (1-M^2) \frac{v}{i\omega} \frac{B_k}{2} (\delta \tilde{f}^- \delta \tilde{g}_0 - \delta \tilde{f}_0 \delta \tilde{g}^-) \right] \\ & - \frac{\delta S_R}{2\gamma A_R} \left\{ \delta f^- \int_{r_s}^r e^{i\omega \int_{R'}^r \frac{1}{1-M^2} \frac{dr}{v}} \right. \\ & \times \frac{\partial}{\partial r} \left[(1-M^2) \frac{v}{i\omega} (A_k \delta \tilde{f}_0 + B_k \delta \tilde{g}_0) \right] dr \\ & - \delta f_0 \int_{\infty}^r e^{i\omega \int_{R'}^r \frac{1}{1-M^2} \frac{dr}{v}} \\ & \left. \times \frac{\partial}{\partial r} \left[(1-M^2) \frac{v}{i\omega} (A_k \delta \tilde{f}^- + B_k \delta \tilde{g}^-) \right] dr \right\} \end{aligned} \quad (\text{C21})$$

Thus

$$A_{k+1} = -\frac{\partial}{\partial r} \left[(1-M^2) \frac{v}{i\omega} A_k \right] - \frac{B_k}{c^2} \left(1 - \frac{\omega_L^2}{\omega^2} \right), \quad (\text{C22})$$

$$B_{k+1} = -\frac{\partial}{\partial r} \left[(1-M^2) \frac{v}{i\omega} B_k \right] - v^2 A_k, \quad (\text{C23})$$

$$D_{k+1} = D_k + (1-M^2) \frac{v}{i\omega} B_k \quad (\text{C24})$$

In consequence,

$$\begin{aligned} A_2 &= \\ & \frac{\partial}{\partial r} \left[(1-M^2) \left(1 - \frac{\omega_L^2}{\omega^2} \right) \right] + \frac{1}{c^2} \left(1 - \frac{\omega_L^2}{\omega^2} \right) \frac{\partial}{\partial r} (c^2 - v^2) \\ & \propto r^{-2}, \end{aligned} \quad (\text{C25})$$

$$\begin{aligned} B_2 &= \frac{\partial}{\partial r} \left[(1-M^2) \frac{v}{i\omega} \frac{\partial}{\partial r} (c^2 - v^2) \right] + i\omega v \left(1 - \frac{\omega_L^2}{\omega^2} \right) \\ & \propto r^{-2}, \end{aligned} \quad (\text{C26})$$

$$D_2 = c^2 - v^2 - (1-M^2) \frac{v}{i\omega} \frac{\partial}{\partial r} (c^2 - v^2) \quad (\text{C27})$$

Noting that $D_k(r_s) = 0$, the limit of this solution at the sonic point is

$$\begin{aligned} \delta f(r_s) &= -\frac{\delta S_R}{2\gamma A_R} \delta f_0(r_s) \\ &\times \int_{\infty}^{r_s} e^{i\omega \int_R^r \frac{1+M^2}{1-M^2} \frac{dr}{v}} (A_k \delta f^- + B_k \delta g^-) dr. \end{aligned} \quad (\text{C28})$$

The energy density in the supersonic region is defined by an equation similar to the subsonic region, using a reference radius $R' < r_s$, the singular function δf_{sup} defined for $r < r_s$ and choosing the boundaries of the integral to ensure the regularity and the continuity across the sonic point:

$$\begin{aligned} \delta f(r < r_s) &= -\frac{\delta S_{R'}}{2\gamma A_R} e^{i\omega \int_{R'}^r \frac{dr}{v}} \delta f_0(r) \\ &\times \int_{\infty}^{r_s} e^{i\omega \int_R^r \frac{1+M^2}{1-M^2} \frac{dr}{v}} (A_k \delta f^- + B_k \delta g^-) dr - \frac{\delta S_{R'}}{2\gamma A_R} \\ &\times \left\{ \delta f_{\text{sup}} \int_{r_s}^r e^{i\omega \int_{R'}^r \frac{1+M^2}{1-M^2} \frac{dr}{v}} \delta f_0 \left(\frac{\partial}{\partial r} \frac{1}{M^2} + \frac{i\omega}{vM^2} \right) dr \right. \\ &\left. - \delta f_0 \int_{r_s}^r e^{i\omega \int_{R'}^r \frac{1+M^2}{1-M^2} \frac{dr}{v}} \delta f_{\text{sup}} \left(\frac{\partial}{\partial r} \frac{1}{M^2} + \frac{i\omega}{vM^2} \right) dr \right\}, \end{aligned} \quad (\text{C29})$$

The pressure perturbation is deduced from equation (A13):

$$\begin{aligned} \delta p(r < r_s) &= -\frac{\delta S_{R'}}{2\gamma A_R} e^{i\omega \int_{R'}^r \frac{dr}{v}} \delta p_0(r) \\ &\int_{\infty}^{r_s} e^{i\omega \int_R^r \frac{1+M^2}{1-M^2} \frac{dr}{v}} (A_k \delta f^- + B_k \delta g^-) dr - \frac{\delta S_{R'}}{2\gamma A_R} \\ &\times \left\{ \delta p_{\text{sup}} \int_{r_s}^r e^{i\omega \int_{R'}^r \frac{1+M^2}{1-M^2} \frac{dr}{v}} \delta f_0 \left(\frac{\partial}{\partial r} \frac{1}{M^2} + \frac{i\omega}{vM^2} \right) dr \right. \\ &\left. - \delta p_0 \int_{r_s}^r e^{i\omega \int_{R'}^r \frac{1+M^2}{1-M^2} \frac{dr}{v}} \delta f_{\text{sup}} \left(\frac{\partial}{\partial r} \frac{1}{M^2} + \frac{i\omega}{vM^2} \right) dr \right\}, \end{aligned} \quad (\text{C30})$$

where δp_0 and δp_{sup} are pressure perturbations corresponding to the homogeneous solution δf_0 and δf_{sup} , respectively. Note that when $r \rightarrow 0$, $M \propto r^{-1/4}$, $c \propto r^{-1/4}$ and $v \propto r^{-1/2}$ for $\gamma = 4/3$,

$$A_1 \equiv -\frac{i\omega}{v} \left(1 - \frac{\omega_l^2}{\omega^2} \right) \propto r^{-\frac{5}{2}}, \quad (\text{C31})$$

$$B_1 \equiv -\frac{\partial}{\partial r} (c^2 - v^2) \propto r^{-2}, \quad (\text{C32})$$

$$D_1 \equiv c^2 - v^2 \propto r^{-1}. \quad (\text{C33})$$

C3 Continuity of the derivative of δf at the sonic point

Continuity of the derivative of δf at the sonic point can be established in the following way. The function δf for advected vorticity perturbations below and above the sonic

point are

$$\begin{aligned} \delta f(r < r_s) &= -\frac{i\delta K_{R'}}{2\omega A_R} \\ &\times \left\{ \delta f_{\text{sup}} \int_{r_s}^r \frac{\delta f_0}{r^2 v} e^{i\omega \int_{R'}^r \frac{1+M^2}{1-M^2} \frac{dr}{v}} dr \right. \\ &- \delta f_0 \int_{r_s}^r \frac{\delta f_{\text{sup}}}{r^2 v} e^{i\omega \int_{R'}^r \frac{1+M^2}{1-M^2} \frac{dr}{v}} dr \\ &\left. - \delta f_0 e^{i\omega \int_{R'}^r \frac{dr}{v}} \int_{\infty}^{r_s} \frac{\delta f^-}{r^2 v} e^{i\omega \int_R^r \frac{1+M^2}{1-M^2} \frac{dr}{v}} dr \right\}. \end{aligned} \quad (\text{C34})$$

$$\begin{aligned} \delta f(r > r_s) &= -\frac{i\delta K_R}{2\omega A_R} \\ &\times \left\{ \delta f^- \int_{r_s}^r e^{i\omega \int_R^r \frac{1+M^2}{1-M^2} \frac{dr}{v}} \frac{\delta f_0}{r^2 v} dr \right. \\ &\left. - \delta f_0 \int_{\infty}^r e^{i\omega \int_R^r \frac{1+M^2}{1-M^2} \frac{dr}{v}} \frac{\delta f^-}{r^2 v} dr \right\}, \end{aligned} \quad (\text{C35})$$

The derivatives of these functions are

$$\begin{aligned} \frac{\partial \delta f}{\partial r}(r < r_s) &= -\frac{i\delta K_{R'}}{2\omega A_R} \\ &\times \left\{ \frac{\partial \delta f_{\text{sup}}}{\partial r} \int_{r_s}^r \frac{\delta f_0}{r^2 v} e^{i\omega \int_{R'}^r \frac{1+M^2}{1-M^2} \frac{dr}{v}} dr \right. \\ &- \frac{\partial \delta f_0}{\partial r} \int_{r_s}^r \frac{\delta f_{\text{sup}}}{r^2 v} e^{i\omega \int_{R'}^r \frac{1+M^2}{1-M^2} \frac{dr}{v}} dr \\ &\left. - \frac{\partial \delta f_0}{\partial r} e^{i\omega \int_{R'}^r \frac{dr}{v}} \int_{\infty}^{r_s} \frac{\delta f^-}{r^2 v} e^{i\omega \int_R^r \frac{1+M^2}{1-M^2} \frac{dr}{v}} dr \right\}. \end{aligned} \quad (\text{C36})$$

$$\begin{aligned} \frac{\partial \delta f}{\partial r}(r > r_s) &= -\frac{i\delta K_R}{2\omega A_R} \\ &\times \left\{ \frac{\partial \delta f^-}{\partial r} \int_{r_s}^r e^{i\omega \int_R^r \frac{1+M^2}{1-M^2} \frac{dr}{v}} \frac{\delta f_0}{r^2 v} dr \right. \\ &\left. - \frac{\partial \delta f_0}{\partial r} \int_{\infty}^r e^{i\omega \int_R^r \frac{1+M^2}{1-M^2} \frac{dr}{v}} \frac{\delta f^-}{r^2 v} dr \right\}. \end{aligned} \quad (\text{C37})$$

We note that the Wronskien of $(\delta f_0, \delta f_{\text{sup}})$ equals that of $(\delta f_0, \delta f^-)$ except for the boundary R or R' .

$$\delta f_0 \frac{\partial f^-}{\partial r} - \delta f^- \frac{\partial f_0}{\partial r} = -\frac{2i\omega A_R v}{1-M^2} e^{-2i\omega \int_{R'}^r \frac{M^2}{1-M^2} \frac{dr}{v}}, \quad (\text{C38})$$

$$\delta f_0 \frac{\partial \delta f_{\text{sup}}}{\partial r} - \delta f_{\text{sup}} \frac{\partial \delta f_0}{\partial r} = -\frac{2i\omega A_R v}{1-M^2} e^{-2i\omega \int_{R'}^r \frac{M^2}{1-M^2} \frac{dr}{v}}. \quad (\text{C39})$$

Thus

$$\frac{\partial \delta f^-}{\partial r} = \frac{\delta f^-}{\delta f_0} \frac{\partial \delta f_0}{\partial r} - \frac{2i\omega A_R v}{1-M^2} \frac{1}{\delta f_0} e^{-2i\omega \int_{R'}^r \frac{M^2}{1-M^2} \frac{dr}{v}}, \quad (\text{C40})$$

$$\frac{\partial \delta f_{\text{sup}}}{\partial r} = \frac{\delta f_{\text{sup}}}{\delta f_0} \frac{\partial \delta f_0}{\partial r} - \frac{2i\omega A_R v}{1-M^2} \frac{1}{\delta f_0} e^{-2i\omega \int_{R'}^r \frac{M^2}{1-M^2} \frac{dr}{v}}. \quad (\text{C41})$$

Using the Wronskien relation, the derivative is rewritten as:

$$\begin{aligned} \frac{\partial \delta f}{\partial r}(r < r_s) &= -\frac{i\delta K_{R'}}{2\omega A_R} \\ &\times \left\{ \left(\frac{\delta f_{\text{sup}}}{\delta f_0} \frac{\partial \delta f_0}{\partial r} - \frac{2i\omega A_R v}{1-M^2} \frac{1}{\delta f_0} e^{-2i\omega \int_{r'}^r \frac{M^2}{1-M^2} \frac{dr}{v}} \right) \right. \\ &\times \int_{r_s}^r \frac{\delta f_0}{r^2 v} e^{i\omega \int_{r'}^r \frac{1+M^2}{1-M^2} \frac{dr}{v}} dr \\ &- \frac{\partial \delta f_0}{\partial r} \int_{r_s}^r \frac{\delta f_{\text{sup}}}{r^2 v} e^{i\omega \int_{r'}^r \frac{1+M^2}{1-M^2} \frac{dr}{v}} dr \\ &\left. - \frac{\partial \delta f_0}{\partial r} e^{i\omega \int_{r'}^r \frac{dr}{v}} \int_{\infty}^{r_s} \frac{\delta f^-}{r^2 v} e^{i\omega \int_R^r \frac{1+M^2}{1-M^2} \frac{dr}{v}} dr \right\}. \quad (\text{C42}) \end{aligned}$$

$$\begin{aligned} \frac{\partial \delta f}{\partial r}(r > r_s) &= -\frac{i\delta K_R}{2\omega A_R} \\ &\times \left\{ \left(\frac{\delta f^-}{\delta f_0} \frac{\partial \delta f_0}{\partial r} - \frac{2i\omega A_R v}{1-M^2} \frac{1}{\delta f_0} e^{-2i\omega \int_R^r \frac{M^2}{1-M^2} \frac{dr}{v}} \right) \right. \\ &\int_{r_s}^r e^{i\omega \int_R^r \frac{1+M^2}{1-M^2} \frac{dr}{v}} \frac{\delta f_0}{r^2 v} dr \\ &\left. - \frac{\partial \delta f_0}{\partial r} \int_{\infty}^r e^{i\omega \int_R^r \frac{1+M^2}{1-M^2} \frac{dr}{v}} \frac{\delta f^-}{r^2 v} dr \right\}. \quad (\text{C43}) \end{aligned}$$

The limit of the derivative at the sonic point

$$\begin{aligned} \frac{\partial \delta f}{\partial r}(r_s^-) &= \frac{i\delta K_{R'}}{2\omega A_R} \\ &\times \left\{ \frac{\partial \delta f_0}{\partial r}(r_s) e^{i\omega \int_{r'}^R \frac{dr}{v}} \int_{\infty}^{r_s} \frac{\delta f^-}{r^2 v} e^{i\omega \int_R^r \frac{1+M^2}{1-M^2} \frac{dr}{v}} dr \right. \\ &+ \frac{2i\omega A_R v}{\delta f_0} \lim_{r \rightarrow r_s^-} \frac{e^{-2i\omega \int_{r'}^r \frac{M^2}{1-M^2} \frac{dr}{v}}}{1-M^2} \\ &\left. \times \int_{r_s}^r \frac{\delta f_0 e^{i\omega \int_{r'}^r \frac{dr}{v}}}{r^2 v} e^{2i\omega \int_{r'}^r \frac{M^2}{1-M^2} \frac{dr}{v}} dr' \right\}. \quad (\text{C44}) \end{aligned}$$

$$\begin{aligned} \frac{\partial \delta f}{\partial r}(r_s^+) &= \frac{i\delta K_R}{2\omega A_R} \\ &\times \left\{ \frac{\partial \delta f_0}{\partial r}(r_s) \int_{\infty}^{r_s} \frac{\delta f^-}{r^2 v} e^{i\omega \int_R^r \frac{1+M^2}{1-M^2} \frac{dr}{v}} dr \right. \\ &+ \frac{2i\omega A_R v}{f_0} \lim_{r \rightarrow r_s^+} \frac{e^{-2i\omega \int_R^r \frac{M^2}{1-M^2} \frac{dr}{v}}}{1-M^2} \\ &\left. \times \int_{r_s}^r \frac{\delta f_0 e^{i\omega \int_R^r \frac{dr}{v}}}{r^2 v} e^{2i\omega \int_R^r \frac{M^2}{1-M^2} \frac{dr}{v}} dr' \right\}, \quad (\text{C45}) \end{aligned}$$

or

$$\begin{aligned} \frac{\partial \delta f}{\partial r}(r_s^-) &= \frac{i\delta K_R}{2\omega A_R} \\ &\times \left\{ \frac{\partial \delta f_0}{\partial r}(r_s) \int_{\infty}^{r_s} \frac{\delta f^-}{r^2 v} e^{i\omega \int_R^r \frac{1+M^2}{1-M^2} \frac{dr}{v}} dr \right. \\ &+ \frac{2i\omega A_R v}{\delta f_0} \lim_{r \rightarrow r_s^-} \frac{1}{1-M^2} \\ &\left. \times \int_{r_s}^r \frac{\delta f_0 e^{i\omega \int_R^r \frac{dr}{v}}}{r^2 v} e^{2i\omega \int_{r'}^r \frac{M^2}{1-M^2} \frac{dr}{v}} dr' \right\}. \quad (\text{C46}) \end{aligned}$$

$$\begin{aligned} \frac{\partial \delta f}{\partial r}(r_s^+) &= \frac{i\delta K_R}{2\omega A_R} \\ &\times \left\{ \frac{\partial \delta f_0}{\partial r}(r_s) \int_{\infty}^{r_s} \frac{\delta f^-}{r^2 v} e^{i\omega \int_R^r \frac{1+M^2}{1-M^2} \frac{dr}{v}} dr \right. \\ &+ \frac{2i\omega A_R v}{\delta f_0} \lim_{r \rightarrow r_s^+} \frac{1}{1-M^2} \\ &\left. \times \int_{r_s}^r \frac{\delta f_0 e^{i\omega \int_R^r \frac{dr}{v}}}{r^2 v} e^{2i\omega \int_{r'}^r \frac{M^2}{1-M^2} \frac{dr}{v}} dr' \right\}, \quad (\text{C47}) \end{aligned}$$

We note that the right and left limit of the last term in the braces are equal:

$$\begin{aligned} &\lim_{x \rightarrow 0^-} \frac{1}{x} \int_0^x e^{i\alpha \log \frac{x'}{x}} dx' \\ &= \frac{1}{x^{1+i\alpha}} \left[\frac{1}{i\alpha+1} (x')^{i\alpha+1} \right]_0^x, \\ &= \frac{1}{i\alpha+1}, \\ &= \lim_{x \rightarrow 0^+} \frac{1}{x} \int_0^x e^{i\alpha \log \frac{x'}{x}} dx' \quad (\text{C48}) \end{aligned}$$

Thus the derivative of δf is continuous across the sonic point. Using a similar procedure, we can prove the continuity of δf for advected entropy waves.

APPENDIX D: CALCULATION OF VORTICITY PARAMETERS

We first establish how components δv_{\perp} and δv_{rot} of velocity decomposition (3) are related to the θ and ϕ components of velocity. For that, we substitute (4) into equation (3):

$$\begin{aligned} \delta \mathbf{v} &= \delta v_r Y_{\ell m} \hat{\mathbf{r}} + \delta v_{\perp} \left(\hat{\theta} \frac{\partial Y_{\ell m}}{\partial \theta} + \hat{\phi} \frac{1}{\sin \theta} \frac{\partial Y_{\ell m}}{\partial \phi} \right) L^{-1} \\ &- \delta v_{\text{rot}} \hat{\mathbf{r}} \times \left(\hat{\theta} \frac{\partial Y_{\ell m}}{\partial \theta} + \hat{\phi} \frac{1}{\sin \theta} \frac{\partial Y_{\ell m}}{\partial \phi} \right) L^{-1} \\ &= \delta v_r Y_{\ell m} \hat{\mathbf{r}} \\ &+ L^{-1} \left[\delta v_{\perp} \frac{\partial Y_{\ell m}}{\partial \theta} + \delta v_{\text{rot}} \frac{1}{\sin \theta} \frac{\partial Y_{\ell m}}{\partial \phi} \right] \hat{\theta} \\ &+ L^{-1} \left[\delta v_{\perp} \frac{1}{\sin \theta} \frac{\partial Y_{\ell m}}{\partial \phi} - \delta v_{\text{rot}} \frac{\partial Y_{\ell m}}{\partial \theta} \right] \hat{\phi}, \quad (\text{D1}) \end{aligned}$$

where we used relations $\hat{\mathbf{r}} \times \hat{\theta} = \hat{\phi}$ and $\hat{\mathbf{r}} \times \hat{\phi} = -\hat{\theta}$. Thus

$$\delta v_{\theta} = L^{-1} \left[\delta v_{\perp} \frac{\partial Y_{\ell m}}{\partial \theta} + \delta v_{\text{rot}} \frac{1}{\sin \theta} \frac{\partial Y_{\ell m}}{\partial \phi} \right], \quad (\text{D2})$$

$$\delta v_{\phi} = L^{-1} \left[\delta v_{\perp} \frac{1}{\sin \theta} \frac{\partial Y_{\ell m}}{\partial \phi} - \delta v_{\text{rot}} \frac{\partial Y_{\ell m}}{\partial \theta} \right]. \quad (\text{D3})$$

A system of differential equations for δv_{θ} and δv_{ϕ} can be obtained by linearizing equation (A1):

$$\frac{\delta v_{\theta}}{v} = \frac{\omega_{\varphi}}{i\omega} + \frac{1}{i\omega v} \frac{\partial}{\partial \theta} \delta f - \frac{c^2}{i\omega v} \frac{\partial}{\partial \theta} \frac{\delta S}{\gamma} e^{i\omega \int_R^r \frac{dr}{v}}, \quad (\text{D4})$$

$$\frac{\delta v_{\phi}}{v} = -\frac{\omega_{\theta}}{i\omega} + \frac{1}{i\omega v \sin \theta} \left[\frac{\partial}{\partial \phi} \delta f - c^2 \frac{\partial}{\partial \phi} \frac{\delta S}{\gamma} e^{i\omega \int_R^r \frac{dr}{v}} \right], \quad (\text{D5})$$

where ω_{θ} and ω_{φ} are the θ and φ components of the vorticity perturbation, which can be obtained from the linearized

vorticity equation (A2) (Kovalenko & Eremin 1998; Foglizzo 2001):

$$\omega_\theta = \frac{1}{rv} \left[Rv_R(\omega_\theta)_R - \frac{c^2 - c_R^2}{\sin\theta} \frac{\partial}{\partial\varphi} \frac{\delta S_R}{\gamma} \right] e^{i\omega \int_R^r \frac{dr}{v}}, \quad (\text{D6})$$

$$\omega_\varphi = \frac{1}{rv} \left[Rv_R(\omega_\varphi)_R + (c^2 - c_R^2) \frac{\partial}{\partial\theta} \frac{\delta S_R}{\gamma} \right] e^{i\omega \int_R^r \frac{dr}{v}}. \quad (\text{D7})$$

Equations (D4) and (D5) can be combined into

$$\frac{r}{\sin\theta} \left[\frac{\partial}{\partial\theta} (\sin\theta\delta v_\theta) + \frac{\partial}{\partial\phi} \delta v_\phi \right] = \frac{1}{i\omega} \left[\delta K - L^2 \delta f \right] Y_{\ell m}, \quad (\text{D8})$$

where $L^2 \equiv l(l+1)$. Using formulas (D2)-(D3), we can obtain

$$\frac{r}{\sin\theta} \left[\frac{\partial}{\partial\theta} (\sin\theta\delta v_\theta) + \frac{\partial}{\partial\phi} \delta v_\phi \right] = -Lr\delta v_\perp Y_{\ell m}. \quad (\text{D9})$$

Combining the last two equations, we obtain an expression for δv_\perp :

$$\delta v_\perp = \frac{L}{i\omega r} \left(\delta f - \frac{\delta K}{L^2} \right). \quad (\text{D10})$$

Next, we decompose the vorticity vector into vector spherical harmonics:

$$\delta\boldsymbol{\omega} = \delta\omega_r Y_{\ell m} \hat{\mathbf{r}} + \delta\omega_\perp L^{-1} \hat{\boldsymbol{\nabla}}_\perp Y_{\ell m} - \delta\omega_{\text{rot}} L^{-1} \hat{\mathbf{r}} \times \hat{\boldsymbol{\nabla}}_\perp Y_{\ell m} \quad (\text{D11})$$

The vorticity perturbation can be calculated as (e.g., Lai & Goldreich 2000)

$$\begin{aligned} \delta\boldsymbol{\omega} &= \nabla \times \delta\mathbf{v} = \frac{L}{r} \delta v_{\text{rot}} Y_{\ell m} \hat{\mathbf{r}} \\ &+ \frac{1}{r} \partial_r (r\delta v_{\text{rot}}) L^{-1} \hat{\boldsymbol{\nabla}}_\perp Y_{\ell m} \\ &- \frac{L\delta v_r - \partial_r(r\delta v_\perp)}{r} L^{-1} \hat{\mathbf{r}} \times \hat{\boldsymbol{\nabla}}_\perp Y_{\ell m}. \end{aligned} \quad (\text{D12})$$

We now apply this formula to calculate the radial component of $\nabla \times \delta\boldsymbol{\omega}$:

$$(\nabla \times \delta\boldsymbol{\omega})_r = \frac{L}{r} \delta\omega_{\text{rot}} Y_{\ell m} \quad (\text{D13})$$

Thus, in the absence of entropy perturbations,

$$\delta K = r^2 v_r (\nabla \times \delta\boldsymbol{\omega})_r = Lr v_r \delta\omega_{\text{rot}} Y_{\ell m}, \quad (\text{D14})$$

which is valid in linear order in the perturbation magnitude. The component $\delta\omega_{\text{rot}}$ can be obtained by comparing equation (D11) and (D12):

$$\delta\omega_{\text{rot}} = \frac{L\delta v_r - \partial_r(r\delta v_\perp)}{r}, \quad (\text{D15})$$

which leads to the following expression for δK

$$\delta K = Lv [L\delta v_r - \partial_r(r\delta v_\perp)] Y_{\ell m}. \quad (\text{D16})$$

APPENDIX E: RELATION BETWEEN THE DIMENSIONLESS ENTROPY AND THE ENTROPY PER NUCLEON

In this section, we derive a relation between the dimensionless entropy that we use and the entropy per nucleon that is usually used in the literature on CCSNe. We use the thermodynamic relation

$$ds = \gamma c_v \left(\frac{dp}{\gamma p} - \frac{d\rho}{\rho} \right), \quad (\text{E1})$$

where ds is the specific entropy and c_v is the specific heat at constant volume. Using the relation

$$c_v = \frac{1}{\mu} \frac{R}{\gamma - 1}, \quad (\text{E2})$$

where R is the universal gas constant and μ is the molar mass, equation (E1) is re-written as

$$ds = \frac{\gamma}{\gamma - 1} \frac{R}{\mu} \left(\frac{dp}{\gamma p} - \frac{d\rho}{\rho} \right). \quad (\text{E3})$$

The entropy is made dimensionless by setting $R/\mu = 1$ without loss of generality:

$$dS = \frac{\gamma}{\gamma - 1} \left(\frac{dp}{\gamma p} - \frac{d\rho}{\rho} \right), \quad (\text{E4})$$

where we used dS to denote the dimensionless entropy. The entropy per nucleon, which we denote as ds_b , is related to the specific entropy ds via

$$ds = \frac{ds_b}{m_b}. \quad (\text{E5})$$

Thus,

$$dS = \frac{ds_b \mu}{R m_b}, \quad (\text{E6})$$

Since

$$\frac{\mu}{R m_b} = \frac{N_A}{R} = \frac{1}{k_b}, \quad (\text{E7})$$

where k_b is the Boltzmann constant, we obtain

$$dS = \frac{ds_b}{k_b}, \quad (\text{E8})$$

which gives us a relation between the dimensionless entropy and the entropy per nucleon.

APPENDIX F: DECOMPOSITION OF HYDRODYNAMIC PERTURBATIONS INTO PHYSICAL COMPONENTS

For uniform inviscid mean flow, the acoustic, entropy, and vorticity perturbations evolve independently from each other in the linear approximation (Kovaszny 1953). However, this is no longer the case for non-uniform background flow. Nevertheless, we can separate the vorticity waves using incompressibility condition, while the in-going and out-going acoustic waves can be separated using the WKB approximation (Foglizzo et al. 2007). In this approach, we decompose perturbations at a given point assuming the perturbations are allowed to evolve in a uniform flow at the same point:

$$\delta f = \delta f^+ + \delta f^- + \delta f^S + \delta f^K, \quad (\text{F1})$$

$$\delta g = \delta g^+ + \delta g^- + \delta g^S + \delta g^K, \quad (\text{F2})$$

where δf^+ and δf^- are the contributions of ingoing and outgoing acoustic waves, while δf^S and δf^K correspond to

δS and δK , which is given as²

$$\delta f^K \equiv \frac{M^2(1-\mu^2)}{1-M^2\mu^2} \frac{\delta K}{L^2}, \quad (\text{F3})$$

$$\delta g^K \equiv \frac{\delta f^K}{v^2} + \delta S, \quad (\text{F4})$$

$$\delta f^S \equiv \frac{c^2(1-M^2)}{1-\mu^2M^2} \frac{\delta S}{\gamma}, \quad (\text{F5})$$

$$\delta g^S \equiv \frac{\mu^2}{c^2} \delta f^S, \quad (\text{F6})$$

$$\delta f^\pm \equiv \frac{1}{2} \delta f \pm \frac{Mc^2}{2\mu} \delta g - \frac{1 \pm \mu M}{2} \left(\delta f^S \pm \frac{\delta f^K}{\mu M} \right), \quad (\text{F7})$$

where

$$\mu^2 \equiv 1 - \frac{L^2 c^2}{\omega^2 r^2} (1 - M^2). \quad (\text{F8})$$

Note that the decomposition of acoustic waves into ingoing and outgoing waves is valid only in the WKB regime where the wavelength of the perturbations is much smaller than the characteristic scale of the background flow. The corresponding values of the perturbations of velocity, density, and pressure are obtained from formulas (A10)-(A13). For vorticity waves, $\delta K \neq 0$ and $\delta S = 0$, which leads to

$$\frac{\delta v_r}{v} = \frac{1}{v^2} \frac{M^2(1-\mu^2)}{1-\mu^2M^2} \frac{\delta K}{L^2}, \quad (\text{F9})$$

$$\frac{\delta v_\perp}{v} = \frac{1}{i\omega r v} \frac{M^2 - 1}{1-\mu^2M^2} \frac{\delta K}{L} \quad (\text{F10})$$

² Foglizzo et al. (2007) uses function h , which related to our function δg through the equation $h \equiv \delta g - \delta S$.

The density and pressure change are zero for vorticity waves in a uniform background flow. For entropy waves, we linearly superpose two solutions with $\delta K = c_R^2 L^2 \delta S / \gamma$ and $\delta S \neq 0$, where R is the initial radius of entropy perturbations. The velocity of the vorticity waves generated by advected entropy perturbations are

$$\frac{\delta v_r}{v} = \frac{1-\mu^2}{1-\mu^2M^2} \left(\frac{c_R^2}{c^2} - 1 \right) \frac{\delta S}{\gamma}, \quad (\text{F11})$$

$$\frac{\delta v_\perp}{v} = \frac{iL}{\omega r v} \frac{1-M^2}{1-\mu^2M^2} (c_R^2 - c^2) \frac{\delta S}{\gamma}. \quad (\text{F12})$$

The associated pressure perturbations is zero because entropy perturbations do not produce pressure variation in a uniform background flow. The associated density perturbations can be obtained from the thermodynamic relation (E1).

In the limit $r \rightarrow 0$, $v \propto r^{-1/2}$ and $c \propto r^{-1/4}$ for $\gamma = 4/3$, which results in $M \propto r^{-1/4}$ and $\mu^2 \propto r^{-3}$. For the velocity field of vorticity waves (F9)-(F10), this results in $\delta v_r \propto r^{1/2}$ and $\delta v_\perp \propto r^2$. For the vorticity waves generated by advected entropy waves (F11)-(F12), we obtain $\delta v_\perp \propto r^{3/2}$ and $\delta v_r \propto \text{const}$.

This paper has been typeset from a $\text{\TeX}/\text{\LaTeX}$ file prepared by the author.